MARCH 06 2019

Bivariate direction finding using two perpendicular bi-directional (“figure-8”) sensors of (possibly) unequal orders

Da Su; Kainam Thomas Wong; Yue Ivan Wu

J. Acoust. Soc. Am. 145, 1241–1258 (2019)
https://doi.org/10.1121/1.5087824

Bivariate direction finding using two perpendicular bi-directional ("figure-8") sensors of (possibly) unequal orders

Da Su,[1] Kainam Thomas Wong,[2] and Yue Ivan Wu[3,a)]
[1]*Department of Electronic and Information Engineering, Hong Kong Polytechnic University, Hong Kong, China*
[2]*School of General Engineering, Beihang University, Beijing 100083, China*
[3]*College of Computer Science, Sichuan University, Chengdu, Sichuan 610065, China*

(Received 2 August 2018; revised 6 December 2018; accepted 2 January 2019; published online 6 March 2019)

A "figure-8" sensor is so labeled because its spatial pattern resembles the character "8" with regard to the sensor's axis. This figure-8 pattern narrows as the sensor's order increases. Using two such figure-8 directional sensors of higher order, oriented perpendicularly to each other—this paper pioneers closed-form signal-processing algorithms to estimate an incident signal's azimuth-elevation bivariate direction-of-arrival. Monte Carlo simulations verify these proposed algorithms' efficacy and statistical closeness to the corresponding Cramér-Rao bounds.
 https://doi.org/10.1121/1.5087824

[MRB] Pages: 1241–1258

I. INTRODUCTION

A. "Figure-8" bi-directional sensors

A "figure-8" sensor is thus called because its directional gain pattern resembles the digit "8," like a dipole, with a mathematical form of $\cos^k(\gamma)$, where $\gamma \in [0,2\pi)$ denotes the incident source's arrival angle (measured with respect to the sensor axis), and where the natural number k refers to the figure-8 sensor's order. A figure-8 sensor is highly directive, enhancing the "random efficiency" (in suppressing background noises/interference that lie off-axis) and extending the "distance factor" (i.e., the sensor's spatial reach on-axis). This gain response is bi-directional, sensitive to incident energy from the back equally as from the front, but with little sideway pickup.

A *first*-order figure-8 sensor (also known as a "pressure gradient" sensor) is often implemented by measuring the pressure difference across two sides of a diaphragm. This represents a first-order finite difference, approximating a spatial derivative of the acoustic pressure's scalar field; hence, such sensors are called "differential sensors." This spatial derivative is proportional to the acoustic particle velocity; hence, the first-order figure-8 sensor is also known as a uniaxial "velocity sensor" or a "velocity hydrophone."

A kth-order figure-8 sensor (Chap. 8.5 of Olson, 1957; Chap. 2.2 of Huang and Benesty, 2004) generalizes the *first*-order figure-8 by measuring the acoustic pressure field at $k + 1$ closely spaced points on a straight line, then computing the kth-order finite difference among them to approximate a measurement of the kth-order partial derivative of the pressure field (Olenko and Wong, 2013, 2015), hence a directional pattern of $\cos^k(\gamma)$. Please refer to Song and Wong (2012) for a brief discussion of higher-order figure-8 sensors.

Figure-8 sensors have been implemented:

(i) First-order figure-8 acoustic sensors are implemented in hardware in Bastyr *et al.* (1999), McConnell *et al.* (2001), and Raangs *et al.* (2001).
(ii) Second-order figure-8 acoustic sensors are implemented in hardware in Brouns (1981), de Bree (2003), Klinke (2003, 2006), Miles (2005), Olson (1941), Rosenfeld (1962), Warren (2008), Warren and Thompson (2003), Wiggins, 1959, 1950, 1951).
(iii) Third-order acoustic sensors are implemented in hardware in Beavers and Brown, (1970), Miles (2005), and Wiggins (1959).
(iv) Fifth-order acoustic sensors are implemented in hardware in Hines *et al.* (2000).
(v) Other higher-order acoustic sensors are implemented in hardware in Miles (2005) and Wiggins (1959).

The above-mentioned hardware implementations of *second*-order or *higher*-order figure-8 sensors date from 1942 to 2008, thereby showing figure-8 sensor technology has been long established yet up-to-date with continuing relevance in practical acoustics.

B. A bi-axial pair of higher-order figure-8 sensors

A pair of first-order figure-8 sensors has long been in practical use for acoustic measurements. It is so common that it has a special name: the "u-u probe." The u-u probe's hardware implementations are discussed in Bastyr *et al.* (1999), McConnell *et al.* (2001), and Raangs *et al.* (2001). The u-u probe's beam patterns and directivity have been studied in de Bree *et al.* (2008) and de Bree and Wind (2010). The u-u probe's closed-form algorithm for azimuth-elevation bivariate direction finding has been proposed in Song *et al.* (2015). This paper will generalize the aforementioned pair of first-order figure-8 sensors to arbitrarily higher orders, where the sensors' orders could be (but do not need to be) unequal.

[a)]Electronic mail: y.i.wu@ieee.org

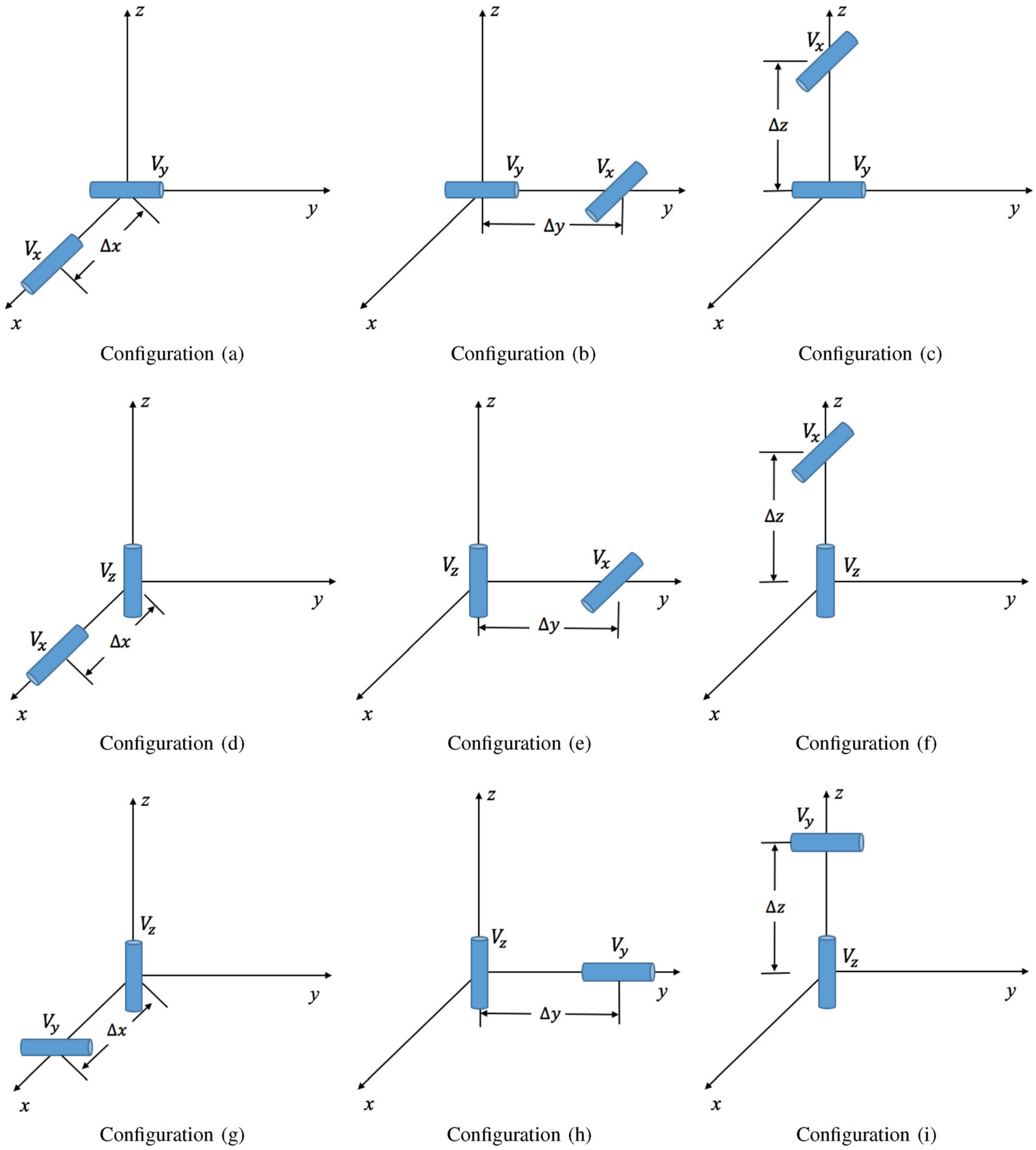

FIG. 1. (Color online) The nine configurations for a pair of figure-8 sensors, oriented orthogonally along some Cartesian axes.

Suppose two figure-8 sensors are oriented orthogonally but each aligned with a different Cartesian coordinate. There would thus be $\binom{3}{2} = 3$ different pairs of coordinates. Further suppose the two sensors are located apart, but their relative displacement is along any one of the three Cartesian coordinates. Then, there would altogether be $3 \times 3 = 9$ different combinations of orientations and displacement. Please see Fig. 1. For each of these nine configurations, this paper will advance new direction-finding algorithms in closed form.

More mathematically: The nine configurations of Fig. 1 may have their 2×1 array manifolds all be symbolized compactly as

$$\mathrm{a}_{\zeta_1,\zeta_2}^{(\epsilon-\text{axis})} = \begin{bmatrix} \eta_1^{k_1} \mathrm{e}^{j2\pi\Delta_\epsilon \mu/\lambda} \\ \eta_2^{k_0} \end{bmatrix}, \tag{1}$$

where

$$\eta_i = \begin{cases} \sin(\theta)\cos(\phi), & \text{if } \zeta_i = x, \\ \sin(\theta)\sin(\phi), & \text{if } \zeta_i = y, \\ \cos(\theta), & \text{if } \zeta_i = z; \end{cases}$$

$$\mu = \begin{cases} \sin(\theta)\cos(\phi), & \text{if } \epsilon = x, \\ \sin(\theta)\sin(\phi), & \text{if } \epsilon = y, \\ \cos(\theta), & \text{if } \epsilon = z. \end{cases}$$

In the above, $\theta \in [0,\pi]$ refers to the polar angle (also known as the zenith angle) measured from the positive z axis, $\phi \in [0, 2\pi)$ denotes the azimuth angle measured from the positive x axis, λ represents the incident signal's wavelength, $\zeta_i \in \{x,y,z\}$ denotes the orientation of ith uniaxial sensor with $i = 1,2$ and $\zeta_1 \neq \zeta_2$, k_0 represents the order of the figure-8 sensor located at the Cartesian origin, k_1 refers to the order of the other figure-8 sensor, the superscript ϵ specifies the displacement axis between two uniaxial sensors, $\mathrm{e}^{j2\pi\Delta_\epsilon\mu/\lambda}$ equals the spatial phase factor introduced by any displacement between the two sensors, Δ_ϵ symbolizes the distance between two constituent sensors, and λ represents the wavelength of the incident signal.[1]

For example, suppose one figure-8 sensor of order k_1 is aligned along the x axis and is placed at $(x,y)=(\Delta_x,0)$, and another figure-8 sensor of order k_0 is aligned along the y axis. This perpendicular pair of figure-8 sensors, of (possibly) unequal orders, has a 2×1 array manifold of

$$\mathbf{a}_{x,y}^{(x-\mathrm{axis})}(\phi) = \begin{bmatrix} [\sin(\theta)\cos(\phi)]^{k_1} e^{j2\pi(\Delta_x/\lambda)\sin(\theta)\cos(\phi)} \\ [\sin(\theta)\sin(\phi)]^{k_0} \end{bmatrix}. \tag{2}$$

These various configurations' array manifolds are interrelated as follows:

$$\mathbf{a}_{x,z}^{(x-\mathrm{axis})}(\theta,\phi) = \mathbf{a}_{y,z}^{(y-\mathrm{axis})}\left(\theta, \phi + \frac{\pi}{2} + 2n\pi\right), \tag{3}$$

$$\mathbf{a}_{x,z}^{(y-\mathrm{axis})}(\theta,\phi) = \mathbf{a}_{y,z}^{(x-\mathrm{axis})}\left(\theta, \phi - \frac{\pi}{2} + 2n\pi\right), \tag{4}$$

$$\mathbf{a}_{x,z}^{(z-\mathrm{axis})}(\theta,\phi) = \mathbf{a}_{y,z}^{(z-\mathrm{axis})}\left(\theta, \phi + \frac{\pi}{2} + 2n\pi\right). \tag{5}$$

Each above identity involves re-aligning an x-oriented directional sensor to become y-oriented or vice versa.

Each configuration realizes spatial resolution in three ways:

(a) the orientation and the length of the spatial displacement between the two sensors;
(b) the order of the first figure-8 sensor;
(c) the order of the second figure-8 sensor.

A higher-order figure-8 sensor has a narrower gain pattern, which results in greater sensitivity toward incident directions more parallel to the sensor's orientation axis. The aforementioned configurations will be compared by their obtainable precision in estimating an incident signal's azimuth-elevation direction-of-arrival (DOA).

C. Organization of this paper

This paper will propose direction-finding formulas in closed forms for each configuration and will derive the corresponding Cramér-Rao bounds (CRBs) to compare across different configurations.

The rest of this paper is organized as follows: Section II will derive new closed-form estimators of an incident signal's azimuth-elevation DOA for the various configurations (a),(b),(d),(f),(h),(i). Section III will do the same for configurations (c),(e),(g). Section IV will present the corresponding CRBs in order to compare the various configurations for their theoretically attainable estimation precision. Section V will present Monte Carlo simulations to verify the proposed estimators' efficacy and statistical closeness to the CRBs. Finally, Sec. VI will conclude the paper.

II. NEW CLOSED-FORM ESTIMATORS OF THE DOA

In eigen-based (also known as "subspace-based") algorithms for parameter estimation, an intermediate step would first estimate each incident source's steering vector. However, this estimate is ambiguous to within a complex-valued multiplicative scalar, unknown to the algorithm. That is, the following is available for the subsequent algorithmic steps of direction finding:

$$\hat{\mathbf{a}}_{\zeta_1,\zeta_2}^{(\epsilon-\mathrm{axis})} \approx c\,\mathbf{a}_{\zeta_1,\zeta_2}^{(\epsilon-\mathrm{axis})}, \tag{6}$$

where c represents a complex-valued scalar.[2]

This unknown c may be eliminated by forming the ratio

$$\frac{\left[\hat{\mathbf{a}}_{\zeta_1,\zeta_2}^{(\epsilon-\mathrm{axis})}\right]_1}{\left[\hat{\mathbf{a}}_{\zeta_1,\zeta_2}^{(\epsilon-\mathrm{axis})}\right]_2} = \frac{\eta_1^{k_1}}{\eta_2^{k_0}} e^{j2\pi(\Delta_\epsilon/\lambda)\mu}, \tag{7}$$

where $[\cdot]_i$ symbolizes the ith element of the vector inside the square brackets.

Equation (7) yields the estimates

$$\widehat{\left(\frac{\eta_1^{k_1}}{\eta_2^{k_0}}\right)} = \left|\frac{\left[\hat{\mathbf{a}}_{\zeta_1,\zeta_2}^{(\epsilon-\mathrm{axis})}\right]_1}{\left[\hat{\mathbf{a}}_{\zeta_1,\zeta_2}^{(\epsilon-\mathrm{axis})}\right]_2}\right| \operatorname{sgn}\left(\frac{\eta_1^{k_1}}{\eta_2^{k_0}}\right), \tag{8}$$

$$\hat{\mu} = \frac{\lambda}{2\pi\Delta_\epsilon} \angle \left(\operatorname{sgn}\left(\frac{\eta_1^{k_1}}{\eta_2^{k_0}}\right) \frac{\left[\hat{\mathbf{a}}_{\zeta_1,\zeta_2}^{(\epsilon-\mathrm{axis})}\right]_1}{\left[\hat{\mathbf{a}}_{\zeta_1,\zeta_2}^{(\epsilon-\mathrm{axis})}\right]_2} \right), \tag{9}$$

where $\operatorname{sgn}(\cdot)$ refers to the sign of the entity inside the parentheses. Equations (8) and (9) require prior knowledge of the sign of $\eta_1^{k_1}/\eta_2^{k_0}$, unless k_1 and k_0 are both even.

The nine configurations in Fig. 1 will have closed-form direction-finding algorithms derived for them in Secs. II A and III below.

The sensors' orders affect the below-proposed algorithms as follows:

- The lower the sensor order, generally, the less computation and the simpler the hardware.
- The prior information required of the source's incident region may be reduced (from one octant to one quadrant of the sphere) if an even order is used.
- For configurations (c),(e),(g)—where the two sensors are oriented differently between them and differently from the inter-sensor displacement—the two sensor's orders must be equal for bivariate direction finding.

For configurations (c),(e),(g), with $k_1 = k_0$, prior information is needed as to which $\frac{1}{4}$ of the sphere from which the source would impinge, whereas the other configurations require such prior knowledge to which $\frac{1}{8}$ of the sphere regardless of k_1 and k_0.[3,4,5]

A. Configuration (a): $\eta_1 = \mu = u$ and $\eta_2 = v$

Here, Eqs. (8) and (9), respectively, become

$$\widehat{\left(\frac{u^{k_1}}{v^{k_0}}\right)} = \overbrace{\left|\frac{\left[\widehat{\mathbf{a}}_{x,y}^{(x-\text{axis})}\right]_1}{\left[\widehat{\mathbf{a}}_{x,y}^{(x-\text{axis})}\right]_2}\right|}^{F_1(k_1,k_0,\theta,\phi):=} \operatorname{sgn}\left(\frac{u^{k_1}}{v^{k_0}}\right),$$

$$\widehat{u} = \overbrace{\frac{\lambda}{2\pi\Delta_x}\angle\left(\operatorname{sgn}\left(\frac{u^{k_1}}{v^{k_0}}\right)\frac{\left[\widehat{\mathbf{a}}_{x,y}^{(x-\text{axis})}\right]_1}{\left[\widehat{\mathbf{a}}_{x,y}^{(x-\text{axis})}\right]_2}\right)}^{F_2(k_1,k_0,\theta,\phi):=}. \tag{10}$$

Straightforward mathematical manipulations give

$$\left|\tan\left(\widehat{\phi}\right)\right| = \left|\widehat{\left(\frac{v}{u}\right)}\right| = \left|\frac{\left(\frac{F_2(k_1,k_0,\theta,\phi)^{k_1}}{F_1(k_1,k_0,\theta,\phi)}\right)^{1/k_0}}{F_2(k_1,k_0,\theta,\phi)}\right|,$$

which results in

$$\tan\left(\widehat{\phi}\right) = \left|\frac{F_2(k_1,k_0,\theta,\phi)^{k_1/k_0-1}}{F_1(k_1,k_0,\theta,\phi)^{1/k_0}}\right| \operatorname{sgn}\left(\frac{v}{u}\right). \tag{11}$$

Assuming $\operatorname{sgn}(v/u)$ is prior known, $\tan(\widehat{\phi})$ can be determined via Eq. (11). Additionally, assuming that $\operatorname{sgn}(u)$ is prior known, $\widehat{\phi}$ in Eq. (11) can be unambiguously determined as

$$\widehat{\phi} = \begin{cases} \frac{\pi}{2}[1-\operatorname{sgn}(u)] + \tan^{-1}\left(\operatorname{sgn}(u)\left|\frac{F_2(k_1,k_0,\theta,\phi)^{k_1/k_0-1}}{F_1(k_1,k_0,\theta,\phi)^{1/k_0}}\right|\right), \\ \quad \text{if } \operatorname{sgn}(v) > 0; \\ \frac{\pi}{2}[3+\operatorname{sgn}(u)] - \tan^{-1}\left(\operatorname{sgn}(u)\left|\frac{F_2(k_1,k_0,\theta,\phi)^{k_1/k_0-1}}{F_1(k_1,k_0,\theta,\phi)^{1/k_0}}\right|\right), \\ \quad \text{if } \operatorname{sgn}(v) < 0. \end{cases} \tag{12}$$

From Eqs. (10) and (12),

$$\sin\left(\widehat{\theta}\right) = \frac{\widehat{u}}{\cos\left(\widehat{\phi}\right)} = F_2(k_1,k_0,\theta,\phi)\sec\left(\widehat{\phi}\right). \tag{13}$$

Assuming that $\operatorname{sgn}(w)$ is prior known, $\widehat{\theta}$ in Eq. (13) can be unambiguously determined as

$$\widehat{\theta} = \begin{cases} \sin^{-1}\left(F_2(k_1,k_0,\theta,\phi)\sec\left(\widehat{\phi}\right)\right), & \text{if } \theta \in \left[0, \frac{\pi}{2}\right); \\ \pi - \sin^{-1}\left(F_2(k_1,k_0,\theta,\phi)\sec\left(\widehat{\phi}\right)\right), & \text{if } \theta \in \left[\frac{\pi}{2}, \pi\right]. \end{cases} \tag{14}$$

B. Configuration (b): $\eta_2 = \mu = v$ and $\eta_1 = u$

Here, Eqs. (8) and (9), respectively, become

$$\widehat{\left(\frac{u^{k_1}}{v^{k_0}}\right)} = \overbrace{\left|\frac{\left[\widehat{\mathbf{a}}_{x,y}^{(y-\text{axis})}\right]_1}{\left[\widehat{\mathbf{a}}_{x,y}^{(y-\text{axis})}\right]_2}\right|}^{F_1(k_1,k_0,\theta,\phi):=} \operatorname{sgn}\left(\frac{u^{k_1}}{v^{k_0}}\right),$$

$$\widehat{v} = \overbrace{\frac{\lambda}{2\pi\Delta_y}\angle\left(\operatorname{sgn}\left(\frac{u^{k_1}}{v^{k_0}}\right)\frac{\left[\widehat{\mathbf{a}}_{x,y}^{(y-\text{axis})}\right]_1}{\left[\widehat{\mathbf{a}}_{x,y}^{(y-\text{axis})}\right]_2}\right)}^{F_2(k_1,k_0,\theta,\phi):=}. \tag{15}$$

Straightforward mathematical manipulations give

$$\left|\tan\left(\widehat{\phi}\right)\right| = \left|\widehat{\left(\frac{v}{u}\right)}\right| = \left|\frac{F_2(k_1,k_0,\theta,\phi)}{\left(F_1(k_1,k_0,\theta,\phi)\,F_2(k_1,k_0,\theta,\phi)^{k_0}\right)^{1/k_1}}\right|,$$

which results in

$$\tan\left(\widehat{\phi}\right) = \left|\frac{F_2(k_1,k_0,\theta,\phi)^{1-k_0/k_1}}{F_1(k_1,k_0,\theta,\phi)^{1/k_1}}\right| \operatorname{sgn}\left(\frac{v}{u}\right). \tag{16}$$

Assuming that $\operatorname{sgn}(v/u)$ is prior known, $\tan(\widehat{\phi})$ can be determined via Eq. (16). Furthermore, assuming that $\operatorname{sgn}(u)$ is prior known, $\widehat{\phi}$ in Eq. (16) can be unambiguously determined as

$$\widehat{\phi} = \begin{cases} \frac{\pi}{2}[1-\operatorname{sgn}(u)] + \tan^{-1}\left(\operatorname{sgn}(u)\left|\frac{F_2(k_1,k_0,\theta,\phi)^{1-k_0/k_1}}{F_1(k_1,k_0,\theta,\phi)^{1/k_1}}\right|\right), \\ \quad \text{if } \operatorname{sgn}(v) > 0; \\ \frac{\pi}{2}[3+\operatorname{sgn}(u)] - \tan^{-1}\left(\operatorname{sgn}(u)\left|\frac{F_2(k_1,k_0,\theta,\phi)^{1-k_0/k_1}}{F_1(k_1,k_0,\theta,\phi)^{1/k_1}}\right|\right), \\ \quad \text{if } \operatorname{sgn}(v) < 0. \end{cases} \tag{17}$$

From Eqs. (15) and (17),

$$\sin\left(\widehat{\theta}\right) = \frac{\widehat{v}}{\sin\left(\widehat{\phi}\right)} = F_2(k_1,k_0,\theta,\phi)\csc\left(\widehat{\phi}\right). \tag{18}$$

Assuming that $\operatorname{sgn}(w)$ is prior known, $\widehat{\theta}$ in Eq. (18) can be unambiguously determined as

$$\widehat{\theta} = \begin{cases} \sin^{-1}\left(F_2(k_1,k_0,\theta,\phi)\csc\left(\widehat{\phi}\right)\right), & \text{if } \theta \in \left[0, \frac{\pi}{2}\right); \\ \pi - \sin^{-1}\left(F_2(k_1,k_0,\theta,\phi)\csc\left(\widehat{\phi}\right)\right), & \text{if } \theta \in \left[\frac{\pi}{2}, \pi\right]. \end{cases} \tag{19}$$

C. Configuration (d): $\eta_1 = \mu = u$ and $\eta_2 = w$

Here, Eqs. (8) and (9), respectively, become

$$\widehat{\left(\frac{u^{k_1}}{w^{k_0}}\right)} = \overbrace{\left|\frac{\left[\hat{\mathbf{a}}_{x,z}^{(x-\text{axis})}\right]_1}{\left[\hat{\mathbf{a}}_{x,z}^{(x-\text{axis})}\right]_2}\right| \text{sgn}\left(\frac{u^{k_1}}{w^{k_0}}\right)}^{F_1(k_1,k_0,\theta,\phi):=},$$

$$\hat{u} = \frac{\lambda}{2\pi\Delta_x}\angle\overbrace{\left(\text{sgn}\left(\frac{u^{k_1}}{w^{k_0}}\right)\frac{\left[\hat{\mathbf{a}}_{x,z}^{(x-\text{axis})}\right]_1}{\left[\hat{\mathbf{a}}_{x,z}^{(x-\text{axis})}\right]_2}\right)}^{F_2(k_1,k_0,\theta,\phi):=}. \tag{20}$$

Straightforward mathematical manipulations give

$$|\cos(\hat{\theta})| = |\hat{w}| = \left|\left(\frac{F_2(k_1,k_0,\theta,\phi)^{k_1}}{F_1(k_1,k_0,\theta,\phi)}\right)^{1/k_0}\right|,$$

which results in

$$\cos(\hat{\theta}) = \left|\frac{F_2(k_1,k_0,\theta,\phi)^{k_1/k_0}}{F_1(k_1,k_0,\theta,\phi)^{1/k_0}}\right|\text{sgn}(w). \tag{21}$$

Assuming that $\text{sgn}(w)$ is prior known, $\cos(\hat{\theta})$ can be determined via Eq. (21). And $\hat{\theta}$ in Eq. (21) can be unambiguously determined as

$$\hat{\theta} = \cos^{-1}\left(\text{sgn}(w)\left|\frac{F_2(k_1,k_0,\theta,\phi)^{k_1/k_0}}{F_1(k_1,k_0,\theta,\phi)^{1/k_0}}\right|\right). \tag{22}$$

From Eqs. (20) and (22),

$$\cos(\hat{\phi}) = \frac{\hat{u}}{\sin(\hat{\theta})} = F_2(k_1,k_0,\theta,\phi)\csc(\hat{\theta}). \tag{23}$$

Assuming $\text{sgn}(v)$ as prior known, $\hat{\phi}$ in Eq. (23) may be unambiguously determined as

$$\hat{\phi} = \begin{cases} \cos^{-1}(F_2(k_1,k_0,\theta,\phi)\csc(\hat{\theta})), & \text{if } \phi \in [0,\pi); \\ 2\pi - \cos^{-1}(F_2(k_1,k_0,\theta,\phi)\csc(\hat{\theta})), & \text{if } \phi \in [\pi, 2\pi). \end{cases} \tag{24}$$

Configuration (h) may be handled similarly.

D. Configuration (f): $\eta_1 = u$ and $\eta_2 = \mu = w$

Here, Eqs. (8) and (9), respectively, become

$$\widehat{\left(\frac{u^{k_1}}{w^{k_0}}\right)} = \overbrace{\left|\frac{\left[\hat{\mathbf{a}}_{x,z}^{(z-\text{axis})}\right]_1}{\left[\hat{\mathbf{a}}_{x,z}^{(z-\text{axis})}\right]_2}\right| \text{sgn}\left(\frac{u^{k_1}}{w^{k_0}}\right)}^{F_1(k_1,k_0,\theta,\phi):=}, \tag{25}$$

$$\hat{w} = \frac{\lambda}{2\pi\Delta_z}\angle\overbrace{\left(\text{sgn}\left(\frac{u^{k_1}}{w^{k_0}}\right)\frac{\left[\hat{\mathbf{a}}_{x,z}^{(z-\text{axis})}\right]_1}{\left[\hat{\mathbf{a}}_{x,z}^{(z-\text{axis})}\right]_2}\right)}^{F_2(k_1,k_0,\theta,\phi):=}. \tag{26}$$

Straightforward mathematical manipulations give

$$\cos(\hat{\theta}) = F_2(k_1,k_0,\theta,\phi). \tag{27}$$

Thus, $\hat{\theta}$ can be unambiguously determined through Eq. (27)

$$\hat{\theta} = \cos^{-1}(F_2(k_1,k_0,\theta,\phi)). \tag{28}$$

From Eqs. (25) and (26),

$$\begin{aligned}|\sin(\hat{\theta})\cos(\hat{\phi})| &= |\hat{u}| \\ &= |(F_1(k_1,k_0,\theta,\phi)F_2(k_1,k_0,\theta,\phi)^{k_0})^{1/k_1}|,\end{aligned}$$

which results in

$$\begin{aligned}\cos(\hat{\phi}) = \text{sgn}(u)\csc(\hat{\theta})|F_1(k_1,k_0,\theta,\phi)^{1/k_1} \\ \times F_2(k_1,k_0,\theta,\phi)^{k_0/k_1}|.\end{aligned} \tag{29}$$

Assuming $\text{sgn}(u)$ as prior known, $\cos(\hat{\phi})$ can be determined via Eq. (29). Moreover, assuming that $\text{sgn}(v)$ is prior known, $\hat{\phi}$ in Eq. (29) can be unambiguously determined as

$$\hat{\phi} = \begin{cases} \cos^{-1}(\text{sgn}(u)\csc(\hat{\theta})|F_1(k_1,k_0,\theta,\phi)^{1/k_1} \\ \quad F_2(k_1,k_0,\theta,\phi)^{k_0/k_1},) \quad \text{if } \phi \in [0,\pi); \\ 2\pi - \cos^{-1}(\text{sgn}(u)\csc(\hat{\theta})|F_1(k_1,k_0,\theta,\phi)^{1/k_1} \\ \quad F_2(k_1,k_0,\theta,\phi)^{k_0/k_1}|), \quad \text{if } \phi \in [\pi, 2\pi). \end{cases}$$

Configuration (i) may be handled analogously.

E. Configurations (c),(e),(g)

Configurations (c), (e), and (g) cannot lead to any closed-form eigen-based direction-finding formula if $k_0 \neq k_1$. These three configurations (and these three alone) have the commonality of η_1 and η_2 and μ being all different, i.e., $\eta_1 \neq \eta_2 \neq \mu \neq \eta_1$.

To see why, consider configuration (e), wherein $\eta_1 = u$, $\eta_2 = w$, and $\mu = v$. Hence,

$$\widehat{\left(\frac{u^{k_1}}{w^{k_0}}\right)} = \overbrace{\left|\frac{\left[\hat{\mathbf{a}}_{x,z}^{(y-\text{axis})}\right]_1}{\left[\hat{\mathbf{a}}_{x,z}^{(y-\text{axis})}\right]_2}\right| \text{sgn}\left(\frac{u^{k_1}}{w^{k_0}}\right)}^{F_1(k_1,k_0,\theta,\phi):=}, \tag{30}$$

$$\hat{v} = \frac{\lambda}{2\pi\Delta_y}\angle\overbrace{\left(\text{sgn}\left(\frac{u^{k_1}}{w^{k_0}}\right)\frac{\left[\hat{\mathbf{a}}_{x,z}^{(y-\text{axis})}\right]_1}{\left[\hat{\mathbf{a}}_{x,z}^{(y-\text{axis})}\right]_2}\right)}^{F_2(k_1,k_0,\theta,\phi):=}. \tag{31}$$

Square both sides of Eq. (30) to give

$$[F_1(k_1,k_0,\theta,\phi)]^2 = \frac{\left(\sin^2(\theta)\cos^2(\phi)\right)^{k_1}}{\left(\cos^2(\theta)\right)^{k_0}} = \frac{\left\{\sin^2(\theta)\left[1-\sin^2(\phi)\right]\right\}^{k_1}}{\left[1-\sin^2(\theta)\right]^{k_0}}. \tag{32}$$

From Eq. (31), $\sin(\phi) = F_2(k_1,k_0,\theta,\phi)/\sin(\theta)$. Substitute $F_2(k_1,k_0,\theta,\phi)/\sin(\theta)$ for $\sin(\phi)$ in Eq. (31) to give

$$[F_1(k_1,k_0,\theta,\phi)]^2 = \frac{\left[\sin^2(\theta)\left(1-\dfrac{F_2(k_1,k_0,\theta,\phi)^2}{\sin^2(\theta)}\right)\right]^{k_1}}{\left[1-\sin^2(\theta)\right]^{k_0}} = \frac{\left[\sin^2(\theta)-F_2(k_1,k_0,\theta,\phi)^2\right]^{k_1}}{\left[1-\sin^2(\theta)\right]^{k_0}}. \tag{33}$$

No closed-form solution exists for this.

Similar difficulties arise for configurations (e) and (g).

III. THE SPECIAL CASE OF $k_0 = k_1 = k$

At $k_0 = k_1 = k$, Eqs. (8) and (9) degenerate to

$$\widehat{\left(\frac{\eta_1}{\eta_2}\right)^k} = \begin{cases} \left|\dfrac{\left[\widehat{\mathbf{a}}^{(\epsilon-\text{axis})}_{\zeta_1,\zeta_2}\right]_1}{\left[\widehat{\mathbf{a}}^{(\epsilon-\text{axis})}_{\zeta_1,\zeta_2}\right]_2}\right| \operatorname{sgn}\left(\dfrac{\eta_1}{\eta_2}\right), & \text{if } k \text{ is odd}, \\ \left|\dfrac{\left[\widehat{\mathbf{a}}^{(\epsilon-\text{axis})}_{\zeta_1,\zeta_2}\right]_1}{\left[\widehat{\mathbf{a}}^{(\epsilon-\text{axis})}_{\zeta_1,\zeta_2}\right]_2}\right|, & \text{if } k \text{ is even}; \end{cases}$$

$$\widehat{\mu} = \begin{cases} \dfrac{1}{2\pi}\dfrac{\lambda}{\Delta_\epsilon}\angle\left(\operatorname{sgn}\left(\dfrac{\eta_1}{\eta_2}\right)\dfrac{\left[\widehat{\mathbf{a}}^{(\epsilon-\text{axis})}_{\zeta_1,\zeta_2}\right]_1}{\left[\widehat{\mathbf{a}}^{(\epsilon-\text{axis})}_{\zeta_1,\zeta_2}\right]_2}\right), & \text{if } k \text{ is odd}, \\ \dfrac{1}{2\pi}\dfrac{\lambda}{\Delta_\epsilon}\angle\left(\dfrac{\left[\widehat{\mathbf{a}}^{(\epsilon-\text{axis})}_{\zeta_1,\zeta_2}\right]_1}{\left[\widehat{\mathbf{a}}^{(\epsilon-\text{axis})}_{\zeta_1,\zeta_2}\right]_2}\right), & \text{if } k \text{ is even}. \end{cases}$$

Table I shows the closed-form formulas for azimuth and elevation angle estimation using configuration (c), (e), and (g) at $k_0 = k_1 = k$. The estimators of ϕ and θ for the other six configurations—(a),(b),(d),(f),(h),(i)—can be deduced from Table II by setting $k_1 = k_0 = k$.

A. Configuration (c): $\eta_1 = u$ and $\eta_2 = v$ and $\mu = w$

For this configuration, the estimation of ϕ and θ is not possible when $k_1 \neq k_0$, as shown in Sec. II E. However, when $k_1 = k_0 = k$, Eqs. (8) and (9) would give

TABLE I. DOA estimation formulas applicable for $k_1 = k_0 = k$.

Configuration	DOA estimation formulas	Prior information required
(c)	$\widehat{\phi} = \begin{cases} \frac{\pi}{2}[1-\operatorname{sgn}(u)] + \tan^{-1}\left(\operatorname{sgn}(u)\lvert F_1(k,\theta,\phi)^{-1/k}\rvert\right), & \text{if } \operatorname{sgn}(v) > 0; \\ \frac{\pi}{2}[3+\operatorname{sgn}(u)] - \tan^{-1}\left(\operatorname{sgn}(u)\lvert F_1(k,\theta,\phi)^{-1/k}\rvert\right), & \text{if } \operatorname{sgn}(v) < 0. \end{cases}$ $\widehat{\theta} = \cos^{-1}(F_2(k,\theta,\phi))$	$\phi \in \left[0,\frac{\pi}{2}\right)$ vs $\left[\frac{\pi}{2},\pi\right)$ vs $\left[\pi,\frac{3\pi}{2}\right)$ vs $\left[\frac{3\pi}{2},2\pi\right)$
(e)	$\widehat{\phi} = \begin{cases} \pi[1-\operatorname{sgn}(\chi^{\text{a}})-\delta(\chi)] + \sin^{-1}\left(\csc(\widehat{\theta})F_2(k,\theta,\phi)\right), & \text{if } \operatorname{sgn}(u) > 0; \\ \pi - \sin^{-1}\left(\csc(\widehat{\theta})F_2(k,\theta,\phi)\right), & \text{if } \operatorname{sgn}(u) < 0. \end{cases}$ $\widehat{\theta} = \begin{cases} \sin^{-1}\left(\sqrt{\frac{F_1(k,\theta,\phi)^{2/k}+F_2(k,\theta,\phi)^2}{1+F_1(k,\theta,\phi)^{2/k}}}\right), & \text{if } \operatorname{sgn}(w) > 0; \\ \pi - \sin^{-1}\left(\sqrt{\frac{F_1(k,\theta,\phi)^{2/k}+F_2(k,\theta,\phi)^2}{1+F_1(k,\theta,\phi)^{2/k}}}\right), & \text{if } \operatorname{sgn}(w) < 0. \end{cases}$ ${}^{\text{a}}\chi = \sin^{-1}\left(\frac{\lambda}{2\pi\Delta_y}\csc(\widehat{\theta})\angle\left(\operatorname{sgn}\left(\frac{u^k}{w^k}\right)\frac{\left[\widehat{\mathbf{a}}^{(y-\text{axis})}_{x,z}\right]_1}{\left[\widehat{\mathbf{a}}^{(y-\text{axis})}_{x,z}\right]_2}\right)\right)$ and $\delta(\chi) = \begin{cases} 1, & \text{if } \chi = 0 \\ 0, & \text{if } \chi \neq 0 \end{cases}$	$\phi \in \left[-\frac{\pi}{2},\frac{\pi}{2}\right)$ vs $\left[\frac{\pi}{2},\frac{3\pi}{2}\right)$ $\theta \in \left[0,\frac{\pi}{2}\right)$ vs $\left[\frac{\pi}{2},\pi\right]$
(g)	$\widehat{\phi} = \begin{cases} \cos^{-1}\left(\csc(\widehat{\theta})F_2(k,\theta,\phi)\right), & \text{if } \operatorname{sgn}(v) > 0; \\ 2\pi - \cos^{-1}\left(\csc(\widehat{\theta})F_2(k,\theta,\phi)\right), & \text{if } \operatorname{sgn}(v) < 0. \end{cases}$ $\widehat{\theta} = \begin{cases} \sin^{-1}\left(\sqrt{\frac{F_1(k,\theta,\phi)^{2/k}+F_2(k,\theta,\phi)^2}{1+F_1(k,\theta,\phi)^{2/k}}}\right), & \text{if } \operatorname{sgn}(w) > 0; \\ \pi - \sin^{-1}\left(\sqrt{\frac{F_1(k,\theta,\phi)^{2/k}+F_2(k,\theta,\phi)^2}{1+F_1(k,\theta,\phi)^{2/k}}}\right), & \text{if } \operatorname{sgn}(w) < 0. \end{cases}$	$\phi \in [0,\pi)$ vs $[\pi,2\pi)$ $\theta \in \left[0,\frac{\pi}{2}\right)$ vs $\left[\frac{\pi}{2},\pi\right]$

TABLE II. DOA estimation formulas applicable for any k_1 and k_0.

Configuration	DOA estimation formulas	Prior information required
(a)	$\widehat{\phi} = \begin{cases} \frac{\pi}{2}[1-\mathrm{sgn}(u)] + \tan^{-1}\left(\mathrm{sgn}(u)\left\lvert \frac{F_2(k_1,k_0,\theta,\phi)^{k_1/k_0-1}}{F_1(k_1,k_0,\theta,\phi)^{1/k_0}}\right\rvert\right), & \text{if } \mathrm{sgn}(v) > 0; \\ \frac{\pi}{2}[3+\mathrm{sgn}(u)] - \tan^{-1}\left(\mathrm{sgn}(u)\left\lvert \frac{F_2(k_1,k_0,\theta,\phi)^{k_1/k_0-1}}{F_1(k_1,k_0,\theta,\phi)^{1/k_0}}\right\rvert\right), & \text{if } \mathrm{sgn}(v) < 0. \end{cases}$ $\widehat{\theta} = \begin{cases} \sin^{-1}\left(F_2(k_1,k_0,\theta,\phi)\sec(\widehat{\phi})\right), & \text{if } \theta \in \left[0,\frac{\pi}{2}\right); \\ \pi - \sin^{-1}\left(F_2(k_1,k_0,\theta,\phi)\sec(\widehat{\phi})\right), & \text{if } \theta \in \left[\frac{\pi}{2},\pi\right]. \end{cases}$	$\phi \in \left[0,\frac{\pi}{2}\right)$ vs $\left[\frac{\pi}{2},\pi\right)$ vs $\left[\pi,\frac{3\pi}{2}\right)$ vs $\left[\frac{3\pi}{2},2\pi\right)$, $\theta \in \left[0,\frac{\pi}{2}\right)$ or $\left[\frac{\pi}{2},\pi\right]$
(b)	$\widehat{\phi} = \begin{cases} \frac{\pi}{2}[1-\mathrm{sgn}(u)] + \tan^{-1}\left(\mathrm{sgn}(u)\left\lvert \frac{F_2(k_1,k_0,\theta,\phi)^{1-k_0/k_1}}{F_1(k_1,k_0,\theta,\phi)^{1/k_1}}\right\rvert\right), & \text{if } \mathrm{sgn}(v) > 0; \\ \frac{\pi}{2}[3+\mathrm{sgn}(u)] - \tan^{-1}\left(\mathrm{sgn}(u)\left\lvert \frac{F_2(k_1,k_0,\theta,\phi)^{1-k_0/k_1}}{F_1(k_1,k_0,\theta,\phi)^{1/k_1}}\right\rvert\right), & \text{if } \mathrm{sgn}(v) < 0. \end{cases}$ $\widehat{\theta} = \begin{cases} \sin^{-1}\left(F_2(k_1,k_0,\theta,\phi)\csc(\widehat{\phi})\right), & \text{if } \theta \in \left[0,\frac{\pi}{2}\right); \\ \pi - \sin^{-1}\left(F_2(k_1,k_0,\theta,\phi)\csc(\widehat{\phi})\right), & \text{if } \theta \in \left[\frac{\pi}{2},\pi\right]. \end{cases}$	$\phi \in \left[0,\frac{\pi}{2}\right)$ vs $\left[\frac{\pi}{2},\pi\right)$ vs $\left[\pi,\frac{3\pi}{2}\right)$ vs $\left[\frac{3\pi}{2},2\pi\right)$, $\theta \in \left[0,\frac{\pi}{2}\right)$ vs $\left[\frac{\pi}{2},\pi\right]$
(d)	$\widehat{\phi} = \begin{cases} \cos^{-1}\left(F_2(k_1,k_0,\theta,\phi)\csc(\widehat{\theta})\right), & \text{if } \phi \in [0,\pi); \\ 2\pi - \cos^{-1}\left(F_2(k_1,k_0,\theta,\phi)\csc(\widehat{\theta})\right), & \text{if } \phi \in [\pi,2\pi). \end{cases}$ $\widehat{\theta} = \cos^{-1}\left(\mathrm{sgn}(w)\left\lvert \frac{F_2(k_1,k_0,\theta,\phi)^{k_1/k_0}}{F_1(k_1,k_0,\theta,\phi)^{1/k_0}}\right\rvert\right)$	If k_1 is odd : $\phi \in \left[0,\frac{\pi}{2}\right)$ vs $\left[\frac{\pi}{2},\pi\right)$ vs $\left[\pi,\frac{3\pi}{2}\right)$ vs $\left[\frac{3\pi}{2},2\pi\right)$, $\theta \in \left[0,\frac{\pi}{2}\right)$ vs $\left[\frac{\pi}{2},\pi\right]$ If k_1 is even : $\phi \in [0,\pi)$ vs $[\pi,2\pi)$, $\theta \in \left[0,\frac{\pi}{2}\right)$ vs $\left[\frac{\pi}{2},\pi\right]$
(f)	$\widehat{\phi} = \begin{cases} \cos^{-1}(\mathrm{sgn}(u)\csc(\widehat{\theta})\lvert F_1(k_1,k_0,\theta,\phi)^{1/k_1}F_2(k_1,k_0,\theta,\phi)^{k_0/k_1}\rvert), & \text{if } \phi \in [0,\pi); \\ 2\pi - \cos^{-1}(\mathrm{sgn}(u)\csc(\widehat{\theta})\lvert F_1(k_1,k_0,\theta,\phi)^{1/k_1}F_2(k_1,k_0,\theta,\phi)^{k_0/k_1}\rvert), & \text{if } \phi \in [\pi,2\pi). \end{cases}$ $\widehat{\theta} = \cos^{-1}(F_2(k_1,k_0,\theta,\phi))$	If k_0 is odd : $\phi \in \left[0,\frac{\pi}{2}\right)$ vs $\left[\frac{\pi}{2},\pi\right)$ vs $\left[\pi,\frac{3\pi}{2}\right)$ vs $\left[\frac{3\pi}{2},2\pi\right)$, $\theta \in \left[0,\frac{\pi}{2}\right)$ vs $\left[\frac{\pi}{2},\pi\right]$ If k_0 is even : $\phi \in \left[0,\frac{\pi}{2}\right)$ vs $\left[\frac{\pi}{2},\pi\right)$ vs $\left[\pi,\frac{3\pi}{2}\right)$ vs $\left[\frac{3\pi}{2},2\pi\right)$

TABLE II. (*Continued*)

Configuration	DOA estimation formulas	Prior information required
(h)	$\widehat{\phi} = \begin{cases} \pi[1-\mathrm{sgn}(\psi^{a})-\delta(\psi)] + \sin^{-1}\Big(F_2(k_1,k_0,\theta,\phi)\csc(\widehat{\theta})\Big), & \text{if} \quad \phi \in \Big[0,\frac{\pi}{2}\Big) \cup \Big[\frac{3\pi}{2},2\pi\Big); \\ \pi - \sin^{-1}\Big(F_2(k_1,k_0,\theta,\phi)\csc(\widehat{\theta})\Big), & \text{if} \quad \phi \in \Big[\frac{\pi}{2},\frac{3\pi}{2}\Big). \end{cases}$ $\widehat{\theta} = \cos^{-1}\left(\mathrm{sgn}(w)\left\vert\frac{F_2(k_1,k_0,\theta,\phi)^{k_1/k_0}}{F_1(k_1,k_0,\theta,\phi)^{1/k_0}}\right\vert\right)$	If k_1 is odd : $\phi \in \Big[0,\frac{\pi}{2}\Big)$ vs $\Big[\frac{\pi}{2},\pi\Big)$ vs $\Big[\pi,\frac{3\pi}{2}\Big)$vs. $\Big[\frac{3\pi}{2},2\pi\Big)$, $\theta \in \Big[0,\frac{\pi}{2}\Big)$ vs $\Big[\frac{\pi}{2},\pi\Big]$ If k_1 is even : $\phi \in \Big[0,\frac{\pi}{2}\Big) \cup \Big[\frac{3\pi}{2},2\pi\Big)$ vs $\Big[\frac{\pi}{2},\frac{3\pi}{2}\Big)$, $\theta \in \Big[0,\frac{\pi}{2}\Big)$ vs $\Big[\frac{\pi}{2},\pi\Big]$
	[a]$\psi = \sin^{-1}\left(\frac{\lambda}{2\pi\Delta_y}\csc(\widehat{\theta})\angle\left(\mathrm{sgn}\left(\frac{v^{k_1}}{w^{k_0}}\right)\frac{\Big[\widehat{\mathbf{a}}_{y,z}^{(y-\text{axis})}\Big]_1}{\Big[\widehat{\mathbf{a}}_{y,z}^{(y-\text{axis})}\Big]_2}\right)\right)$ and $\delta(\psi) = \begin{cases} 1, & \text{if } \psi = 0 \\ 0, & \text{if } \psi \neq 0. \end{cases}$	
(i)	$\widehat{\phi} = \begin{cases} \pi[1-\mathrm{sgn}(v)-\delta(v)] + \sin^{-1}\Big(\mathrm{sgn}(v)\csc(\widehat{\theta})\vert F_1(k_1,k_0,\theta,\phi)^{1/k_1}F_2(k_1,k_0,\theta,\phi)^{k_0/k_1}\vert\Big), \\ \text{if} \quad \phi \in \Big[0,\frac{\pi}{2}\Big) \cup \Big[\frac{3\pi}{2},2\pi\Big); \\ \pi - \sin^{-1}\Big(\mathrm{sgn}(v)\csc(\widehat{\theta})\vert F_1(k_1,k_0,\theta,\phi)^{1/k_1}F_2(k_1,k_0,\theta,\phi)^{k_0/k_1}\vert\Big), \ \text{if } \phi \in \Big[\frac{\pi}{2},\frac{3\pi}{2}\Big). \end{cases}$ $\widehat{\theta} = \cos^{-1}\left(\mathrm{sgn}(w)\left\vert\frac{F_2(k_1,k_0,\theta,\phi)^{k_1/k_0}}{F_1(k_1,k_0,\theta,\phi)^{1/k_0}}\right\vert\right)$	If k_0 is odd : $\phi \in \Big[0,\frac{\pi}{2}\Big)$ vs $\Big[\frac{\pi}{2},\pi\Big)$ vs $\Big[\pi,\frac{3\pi}{2}\Big)$ vs $\Big[\frac{3\pi}{2},2\pi\Big)$, $\theta \in \Big[0,\frac{\pi}{2}\Big)$ vs $\Big[\frac{\pi}{2},\pi\Big]$ If k_0 is even : $\phi \in \Big[0,\frac{\pi}{2}\Big)$ vs $\Big[\frac{\pi}{2},\pi\Big)$ vs $\Big[\pi,\frac{3\pi}{2}\Big)$ vs $\Big[\frac{3\pi}{2},2\pi\Big)$

$$\widehat{\left(\frac{u}{v}\right)^k} := \overbrace{\left|\frac{\left[\widehat{\mathbf{a}}_{x,y}^{(z-\text{axis})}\right]_1}{\left[\widehat{\mathbf{a}}_{x,y}^{(z-\text{axis})}\right]_2}\right|\mathrm{sgn}\left(\frac{u^k}{v^k}\right)}^{F_1(k,\theta,\phi):=},$$

$$\widehat{w} := \overbrace{\frac{\lambda}{2\pi\Delta_z}\angle\left(\mathrm{sgn}\left(\frac{u^k}{v^k}\right)\frac{\left[\widehat{\mathbf{a}}_{x,y}^{(z-\text{axis})}\right]_1}{\left[\widehat{\mathbf{a}}_{x,y}^{(z-\text{axis})}\right]_2}\right)}^{F_2(k,\theta,\phi):=}. \tag{34}$$

Straightforward manipulation gives

$$\left|\tan\left(\widehat{\phi}\right)\right| = \left|\widehat{\left(\frac{v}{u}\right)}\right| = |F_1(k,\theta,\phi)^{-1/k}|,$$

and therefore

$$\tan\left(\widehat{\phi}\right) = |F_1(k,\theta,\phi)^{-1/k}|\mathrm{sgn}\left(\frac{v}{u}\right). \tag{35}$$

Assuming that $\mathrm{sgn}(v/u)$ is prior known, $\tan(\widehat{\phi})$ can be determined via Eq. (35). Additionally, assuming that $\mathrm{sgn}(u)$ is prior known, $\widehat{\phi}$ in Eq. (35) can be unambiguously determined as

$$\widehat{\phi} = \begin{cases} \frac{\pi}{2}[1-\mathrm{sgn}(u)] + \tan^{-1}\left(\mathrm{sgn}(u)|F_1(k,\theta,\phi)^{-1/k}|\right), \\ \quad \text{if } \mathrm{sgn}(v) > 0; \\ \frac{\pi}{2}[3+\mathrm{sgn}(u)] - \tan^{-1}\left(\mathrm{sgn}(u)|F_1(k,\theta,\phi)^{-1/k}|\right), \\ \quad \text{if } \mathrm{sgn}(v) < 0. \end{cases}$$

From Eq. (34),

$$\cos(\widehat{\theta}) = \widehat{w} = F_2(k,\theta,\phi). \tag{36}$$

Thus, $\widehat{\theta}$ in Eq. (36) can be unambiguously determined as

$$\widehat{\theta} = \cos^{-1}(F_2(k,\theta,\phi)). \tag{37}$$

B. Configuration (e): $\eta_1 = u$ and $\eta_2 = w$ and $\mu = v$

For this configuration, the estimation of ϕ and θ is not possible when $k_1 \neq k_0$, as pointed out in Sec. II E. However, when $k_1 = k_0 = k$, from Eqs. (8) and (9)

$$\widehat{\left(\frac{u^{k_1}}{w^{k_0}}\right)} := \overbrace{\left|\frac{\left[\widehat{\mathbf{a}}_{x,z}^{(y-\text{axis})}\right]_1}{\left[\widehat{\mathbf{a}}_{x,z}^{(y-\text{axis})}\right]_2}\right|\mathrm{sgn}\left(\frac{u^k}{w^k}\right)}^{F_1(k,\theta,\phi):=}, \tag{38}$$

$$\widehat{v} := \overbrace{\frac{\lambda}{2\pi\Delta_y}\angle\left(\mathrm{sgn}\left(\frac{u^k}{w^k}\right)\frac{\left[\widehat{\mathbf{a}}_{x,z}^{(y-\text{axis})}\right]_1}{\left[\widehat{\mathbf{a}}_{x,z}^{(y-\text{axis})}\right]_2}\right)}^{F_2(k,\theta,\phi):=}. \tag{39}$$

Straightforward deduction from Eqs. (38) and (39)

$$\begin{aligned} F_1(k,\theta,\phi)^{2/k} &= \frac{\sin^2\left(\widehat{\theta}\right)\cos^2\left(\widehat{\phi}\right)}{\cos^2\left(\widehat{\theta}\right)} \\ &= \frac{\sin^2\left(\widehat{\theta}\right)\left(1-\sin^2\left(\widehat{\phi}\right)\right)}{1-\sin^2\left(\widehat{\theta}\right)} \\ &= \frac{\sin^2\left(\widehat{\theta}\right)\left(1-F_2(k,\theta,\phi)^2/\sin^2\left(\widehat{\theta}\right)\right)}{1-\sin^2\left(\widehat{\theta}\right)} \\ &= \frac{\sin^2\left(\widehat{\theta}\right)-F_2(k,\theta,\phi)^2}{1-\sin^2\left(\widehat{\theta}\right)}; \end{aligned}$$

hence,

$$\sin^2\left(\widehat{\theta}\right) = \frac{F_1(k,\theta,\phi)^{2/k} + F_2(k,\theta,\phi)^2}{1+F_1(k,\theta,\phi)^{2/k}}. \tag{40}$$

As $\theta \in [0,\pi]$, $\sin(\theta) \geq 0$. Thus, Eq. (40) gives

$$\sin\left(\widehat{\theta}\right) = \sqrt{\frac{F_1(k,\theta,\phi)^{2/k} + F_2(k,\theta,\phi)^2}{1+F_1(k,\theta,\phi)^{2/k}}}. \tag{41}$$

Assuming $\mathrm{sgn}(w)$ as prior known, $\widehat{\theta}$ in Eq. (41) can be unambiguously determined as

$$\widehat{\theta} = \begin{cases} \sin^{-1}\left(\sqrt{\frac{F_1(k,\theta,\phi)^{2/k} + F_2(k,\theta,\phi)^2}{1+F_1(k,\theta,\phi)^{2/k}}}\right), \\ \quad \text{if } \mathrm{sgn}(w) > 0; \\ \pi - \sin^{-1}\left(\sqrt{\frac{F_1(k,\theta,\phi)^{2/k} + F_2(k,\theta,\phi)^2}{1+F_1(k,\theta,\phi)^{2/k}}}\right), \\ \quad \text{if } \mathrm{sgn}(w) < 0. \end{cases} \tag{42}$$

From Eqs. (39) and (42),

$$\sin\left(\widehat{\phi}\right) = \frac{\widehat{v}}{\sin\left(\widehat{\theta}\right)} = F_2(k,\theta,\phi)\csc\left(\widehat{\theta}\right). \tag{43}$$

Assuming $\mathrm{sgn}(u)$ as prior known, $\widehat{\phi}$ in Eq. (43) can be unambiguously determined as

$$\widehat{\phi} = \begin{cases} \pi[1-\mathrm{sgn}(\chi)-\delta(\chi)] + \sin^{-1}(\csc(\widehat{\theta})F_2(k,\theta,\phi)), \\ \quad \text{if } \mathrm{sgn}(u) > 0; \\ \pi - \sin^{-1}(\csc(\widehat{\theta})F_2(k,\theta,\phi)), \\ \quad \text{if } \mathrm{sgn}(u) < 0; \end{cases}$$

where

$$\chi = \sin^{-1}\left(\frac{\lambda}{2\pi\Delta_y}\csc\left(\widehat{\theta}\right)\angle\left(\mathrm{sgn}\left(\frac{u^k}{w^k}\right)\frac{\left[\widehat{\mathbf{a}}_{x,z}^{(y-\text{axis})}\right]_1}{\left[\widehat{\mathbf{a}}_{x,z}^{(y-\text{axis})}\right]_2}\right)\right)$$

Configuration (g) may likewise be handled.

IV. CRAMÉR-RAO BOUNDS

Given the statistical data model (i.e., given *how* the observed data are statistically related to the to-be-estimated parameters), any unbiased estimator's error covariance is lower bounded by the CRB.

To focus on the nine configurations in Fig. 1, a simple statistical signal/noise model will be used in the following analysis. More complicated signal/noise models can readily be addressed, using the same analytical approach.

Suppose a pure-tone signal $s(t_n) = \sqrt{P_s}e^{j(2\pi f T_s+\varphi)}$ impinges from the far field upon any of the sensor-pairs in Fig. 1.[6] Here, P_s denotes the signal's unknown power, φ symbolizes the signal's unknown deterministic initial phase, f signifies the signal's prior known frequency, and T_s refers to a time-sampling period that satisfies the Nyquist sampling requirement.

At the mth time instant, a 2×1 data vector would be collected

$$\tilde{\mathbf{z}}(mT_s) = \mathbf{a}_{\zeta_1,\zeta_2}^{(\epsilon-\text{axis})}\, s(mT_s) + \mathbf{n}(mT_s), \tag{44}$$

where $\mathbf{n}(mT_s)$ is the additive noise vector, which is statistical uncorrelated over time and across the two sensors, Gaussian distributed, zero-mean, with an unknown variance of P_n.

With M number of snapshots, the entire dataset may be represented as a $2M \times 1$ vector

$$\begin{aligned}\mathbf{z} :&= \left[\tilde{\mathbf{z}}(T_s)^T, \ldots, \tilde{\mathbf{z}}(MT_s)^T\right]^T \\ &= \underbrace{\mathbf{s} \otimes \mathbf{a}_{\zeta_1,\zeta_2}^{(\epsilon-\text{axis})}}_{\stackrel{\text{def}}{=}\boldsymbol{\mu}} + \underbrace{\left[\tilde{\mathbf{n}}(T_s)^T, \ldots, \tilde{\mathbf{n}}(MT_s)^T\right]}_{\stackrel{\text{def}}{=}\mathbf{n}}.\end{aligned} \tag{45}$$

Here, $\mathbf{s} := \sqrt{P_s}e^{j\varphi}[e^{jT_s\omega}, \ldots, e^{jMT_s\omega}]^T$ represents an $M \times 1$ vector, $\otimes$ symbolizes the Kronecker product, and $\mathbf{n}$ refers to a $2M \times 1$ vector with a covariance matrix $\Gamma = \mathbf{I}_M \otimes \text{diag}(P_n, P_n)$, and $\mathbf{I}_M$ signifies an $M \times M$ identity matrix.

Collect all (deterministic) unknown scalars into a 5×1 vector of $\boldsymbol{\psi} = [\theta, \phi, \varphi, P_s, P_n]^T$. The corresponding 5×5 Fisher information matrix ($\mathbf{J}$) would have an (i,j)th entry of

$$\begin{aligned}[\mathbf{J}]_{i,j} = 2\text{Re}&\left[\left(\frac{\partial \boldsymbol{\mu}}{\partial[\psi]_i}\right)^H \boldsymbol{\Gamma}^{-1}\left(\frac{\partial \boldsymbol{\mu}}{\partial[\psi]_j}\right)\right] \\ &+ \text{Tr}\left[\boldsymbol{\Gamma}^{-1}\frac{\partial \boldsymbol{\Gamma}}{\partial[\psi]_i}\boldsymbol{\Gamma}^{-1}\frac{\partial \boldsymbol{\Gamma}}{\partial[\psi]_j}\right],\end{aligned} \tag{46}$$

where $\text{Tr}[\cdot]$ denotes the trace operator and ^{H} refers to Hermitian transposition.

Then, the bivariate DOA's deterministic/conditional CRBs equal

$$\begin{aligned}\text{CRB}_\theta^{(\cdot)}(\theta,\phi) &= [\mathbf{J}^{-1}]_{1,1}, \\ \text{CRB}_\phi^{(\cdot)}(\theta,\phi) &= [\mathbf{J}^{-1}]_{2,2}.\end{aligned}$$

Table III summarizes all configurations' CRBs. Some qualitative observations thereof:

(i) Each CRB is symmetric.
- (i-1) with respect to $\theta = 90°$ over $\theta \in [0,180°]$,
- (i-2) with respect to $\phi = 180°$ over $\phi \in [0,360°]$,
- (i-3) with respect to $\phi = 90°$ over $\phi \in [0,180°]$, and
- (i-4) with respect to $\phi = 270°$ over $\phi \in [180°,360°]$.

To see the effects of the two figure-8 sensors' respective orders of (k_0,k_1): Fig. 2 compare the polar angle (θ) CRBs for configuration (a) at various (k_0,k_1) under a constraint of $k_0 + k_1 = 4$, i.e., at $(k_1,k_0) = (1,3)$, (2,2), (3,1). Figure 3 does the same for the azimuth angle (ϕ).

(ii) Configuration (a) becomes more sensitive along the x axis (y axis) as $k_1 = k_x$ ($k_0 = k_y$) increases, thereby shifting the CRBs' bases of Figs. 2 and 3 from near $\phi \approx 90°$ toward $\phi \approx 180°$.

(iii) Due to the functional relationship in Eq. (3) between array manifolds of configurations (d) and (h),

$$\begin{aligned}\text{CRB}_\theta^{(\text{d})}(\theta,\phi) &= \text{CRB}_\theta^{(\text{h})}\left(\theta, \phi + \frac{\pi}{2} + 2n\pi\right), \\ \text{CRB}_\phi^{(\text{d})}(\theta,\phi) &= \text{CRB}_\phi^{(\text{h})}\left(\theta, \phi + \frac{\pi}{2} + 2n\pi\right),\end{aligned}$$

where n represents any integer.

Similarly for configurations (e) and (g) on account of the functional relationship in Eq. (4)

$$\begin{aligned}\text{CRB}_\theta^{(\text{e})}(\theta,\phi) &= \text{CRB}_\theta^{(\text{g})}\left(\theta, \phi - \frac{\pi}{2} + 2n\pi\right), \\ \text{CRB}_\phi^{(\text{e})}(\theta,\phi) &= \text{CRB}_\phi^{(\text{g})}\left(\theta, \phi - \frac{\pi}{2} + 2n\pi\right),\end{aligned}$$

Likewise, for configurations (f) and (i) on account of the functional relationship in Eq. (5)

$$\begin{aligned}\text{CRB}_\theta^{(\text{f})}(\theta,\phi) &= \text{CRB}_\theta^{(\text{i})}\left(\theta, \phi + \frac{\pi}{2} + 2n\pi\right), \\ \text{CRB}_\phi^{(\text{f})}(\theta,\phi) &= \text{CRB}_\phi^{(\text{i})}\left(\theta, \phi + \frac{\pi}{2} + 2n\pi\right).\end{aligned}$$

Each pair of identities here involve re-aligning an x-oriented directional sensor to become y-oriented or vice versa.

Figure 4 plots the cumulative histograms of the CRBs for all nine configurations. Because of the equivalence in the six unnumbered equations above, Fig. 4 has only six pairs of graphs. Each cumulative histogram represents the fraction of all possible DOAs at which the estimation would be at least as precise as specified by the abscissa. These cumulated histograms have been evaluated over a 4050-point uniform grid over the unit-sphere's surface. As the CRB represents the best obtainable unbiased estimation error variance, the higher this cumulative histogram the better. Some qualitative observations:

(iv) For configuration (a) [(b)]: the case of $k_0 = k_y = 1[3]$, $k_1 = k_x = 3[1]$ {i.e., the yellow dashed (blue dashed-

TABLE III. CRBs for elevation and azimuth angle estimation using the nine configurations.

Configuration	$2M\frac{P_s}{P_n}\mathrm{CRB}_{\theta}^{(\cdot)}(\theta,\phi)$	$2M\frac{P_s}{P_n}\mathrm{CRB}_{\phi}^{(\cdot)}(\theta,\phi)$
(a)	$\frac{(u(\theta,\phi)^{2k_1\,\mathrm{a}}+v(\theta,\phi)^{2k_0\,\mathrm{b}})\left[\left(2\pi\frac{\Delta_\epsilon}{\lambda}\right)^2 u(\theta,\phi)^2\sin^4(\phi)+(k_1^2+k_0^2)\cos^4(\phi)-{k_1}^2\cos(2\phi)+2k_1k_0\cos^2(\phi)\sin^2(\phi)\right]}{\left(2\pi\frac{\Delta_\epsilon}{\lambda}\right)^2 {k_0}^2\, u(\theta,\phi)^{2k_1}\, v(\theta,\phi)^{2k_0}\cos^2(\theta)\cos^2(\phi)}$	$\frac{(u(\theta,\phi)^{2k_1}+v(\theta,\phi)^{2k_0})\left(\left(2\pi\frac{\Delta_\epsilon}{\lambda}\right)^2 u(\theta,\phi)^2+(k_1-k_0)^2\right)\sin^2(\phi)}{\left(2\pi\frac{\Delta_\epsilon}{\lambda}\right)^2 {k_0}^2\, u(\theta,\phi)^{2k_1}\, v(\theta,\phi)^{2k_0}\sin^2(\theta)}$
(b)	$\frac{(u(\theta,\phi)^{2k_1}+v(\theta,\phi)^{2k_0})\left[\left(2\pi\frac{\Delta_\epsilon}{\lambda}\right)^2 u(\theta,\phi)^2\cos^2(\phi)\sin^2(\phi)+(k_1-k_0)^2\cos(\phi)^4-{k_1}^2\cos(2\phi)+2k_1k_0\cos^2(\phi)\right]}{\left(2\pi\frac{\Delta_\epsilon}{\lambda}\right)^2 {k_1}^2\, u(\theta,\phi)^{2k_1}\, v(\theta,\phi)^{2k_0}\cos^2(\theta)\sin^2(\phi)}$	$\frac{\cos^2(\phi)(u(\theta,\phi)^{2k_1}+v(\theta,\phi)^{2k_0})\left(\left(2\pi\frac{\Delta_\epsilon}{\lambda}\right)^2 v(\theta,\phi)^2+(k_1-k_0)^2\right)}{\left(2\pi\frac{\Delta_\epsilon}{\lambda}\right)^2 {k_1}^2\, u(\theta,\phi)^{2k_1}\, v(\theta,\phi)^{2k_0}\sin^2(\theta)}$
(c)	$\frac{u(\theta,\phi)^{2k}+v(\theta,\phi)^{2k}}{\left(2\pi\frac{\Delta_\epsilon}{\lambda}\right)^2 u(\theta,\phi)^{2k}\, v(\theta,\phi)^{2k}\sin^2(\theta)}$	$\frac{\cos^2(\phi)\sin^2(\phi)(u(\theta,\phi)^{2k}+v(\theta,\phi)^{2k})\left(2\pi\frac{\Delta_\epsilon}{\lambda}\right)^2}{\left(2\pi\frac{\Delta_\epsilon}{\lambda}\right)^2 k^2\, u(\theta,\phi)^{2k}\, v(\theta,\phi)^{2k}}$
(d)	$\frac{\cos^{2-2k_0}(\theta)(\cos^{2k_0}(\theta)+u(\theta,\phi)^{2k_1})\left(\left(2\pi\frac{\Delta_\epsilon}{\lambda}\right)^2 u(\theta,\phi)^2+{k_1}^2\right)}{d^2\,{k_0}^2\, u(\theta,\phi)^{2k_1+2}\sin^2(\theta)}$	$\frac{(\cos^{2k_0}(\theta)+u(\theta,\phi)^{2k_1})\left[\left(2\pi\frac{\Delta_\epsilon}{\lambda}\right)^2 u(\theta,\phi)^2\cos^4(\theta)+(k_1-k_0)^2\cos^4(\theta)+2k_1k_0\cos^2(\theta)-{k_0}^2\cos(2\theta)\right]}{\left(2\pi\frac{\Delta_\epsilon}{\lambda}\right)^2 {k_0}^2 u(\theta,\phi)^{2k_1}\, v(\theta,\phi)^2\sin^4(\theta)\cos^{2k_0}(\theta)}$
(e)	$\frac{\cos^{2-2k}(\theta)(\cos^{2k}(\theta)+u(\theta,\phi)^{2k})\left(\left(2\pi\frac{\Delta_\epsilon}{\lambda}\right)^2 u(\theta,\phi)^2\cos^2(\phi)+k^2\sin^2(\phi)\right)}{\left(2\pi\frac{\Delta_\epsilon}{\lambda}\right)^2 u(\theta,\phi)^{2k}\left(k\,u(\theta,\phi)^2+k\cos^2(\theta)\right)^2}$	$\frac{\cos^2(\phi)(\cos^{2k}(\theta)+u(\theta,\phi)^{2k})\left(\left(2\pi\frac{\Delta_\epsilon}{\lambda}\right)^2 v(\theta,\phi)^2\cos^4(\theta)+k^2\right)}{\left(2\pi\frac{\Delta_\epsilon}{\lambda}\right)^2 u(\theta,\phi)^{2k}\sin^2(\theta)\cos^{2k}(\theta)\left(k\,u(\theta,\phi)^2+k\cos^2(\theta)\right)^2}$
(f)	$\frac{\cos^{2k_0}(\theta)+u(\theta,\phi)^{2k_1}}{\left(2\pi\frac{\Delta_\epsilon}{\lambda}\right)^2 u(\theta,\phi)^{2k_1}\sin^2(\theta)\cos^{2k_0}(\theta)}$	$\frac{\cos^2(\phi)(\cos^{2k_0}(\theta)+u(\theta,\phi)^{2k_1})\left[\left(2\pi\frac{\Delta_\epsilon}{\lambda}\right)^2 \cos^2(\theta)\sin^4(\theta)+(k_1-k_0)^2\cos^4(\theta)+2k_1k_0\cos^2(\theta)-{k_0}^2\cos(2\theta)\right]}{\left(2\pi\frac{\Delta_\epsilon}{\lambda}\right)^2 {k_1}^2\, u(\theta,\phi)^{2k_1}\, v(\theta,\phi)^2\sin^2(\theta)\cos^{2k_0+2}(\theta)}$
(g)	$\frac{\cos^{2-2k}(\theta)(\cos^{2k}(\theta)+v(\theta,\phi)^{2k})\left(\left(2\pi\frac{\Delta_\epsilon}{\lambda}\right)^2 v(\theta,\phi)^2\sin^2(\phi)+k^2\cos^2(\phi)\right)}{\left(2\pi\frac{\Delta_\epsilon}{\lambda}\right)^2 v(\theta,\phi)^{2k}\left(k\,v(\theta,\phi)^2+k\cos^2(\theta)\right)^2}$	$\frac{\sin^2(\phi)(\cos^{2k}(\theta)+v(\theta,\phi)^{2k})\left(k^2+\left(2\pi\frac{\Delta_\epsilon}{\lambda}\right)^2 u(\theta,\phi)^2\cos^4(\theta)\right)}{\left(2\pi\frac{\Delta_\epsilon}{\lambda}\right)^2 v(\theta,\phi)^{2k}\sin^2(\theta)\cos^{2k}(\theta)\left(kv(\theta,\phi)^2+k\cos^2(\theta)\right)^2}$
(h)	$\frac{\cos^{2-2k_0}(\theta)(\cos^{2k_0}(\theta)+v(\theta,\phi)^{2k_1})\left(\left(2\pi\frac{\Delta_\epsilon}{\lambda}\right)^2 v(\theta,\phi)^2+{k_1}^2\right)}{\left(2\pi\frac{\Delta_\epsilon}{\lambda}\right)^2 {k_0}^2\, v(\theta,\phi)^{2k_1+2}\sin^2(\theta)}$	$\frac{(\cos^{2k_0}(\theta)+v(\theta,\phi)^{2k_1})\left[\left(k_1\cos^2(\theta)+k_0\sin^2(\theta)\right)^2+\left(2\pi\frac{\Delta_\epsilon}{\lambda}\right)^2 v(\theta,\phi)^2\cos^4(\theta)\right]}{\left(2\pi\frac{\Delta_\epsilon}{\lambda}\right)^2 {k_0}^2\, u(\theta,\phi)^2\, v(\theta,\phi)^{2k_1}\sin^4(\theta)\cos^{2k_0}(\theta)}$
(i)	$\frac{\cos^{2k_0}(\theta)+v(\theta,\phi)^{2k_1}}{\left(2\pi\frac{\Delta_\epsilon}{\lambda}\right)^2 v(\theta,\phi)^{2k_1}\sin^2(\theta)\cos^{2k_0}(\theta)}$	$\frac{\sin^2(\phi)\left(\cos^{2k_0}(\theta)+v(\theta,\phi)^{2k_1}\right)\left[(k_1\cos^2(\theta)+k_0\sin^2(\theta))^2+\left(2\pi\frac{\Delta_\epsilon}{\lambda}\right)^2\sin^4(\theta)\cos^2(\theta)\right]}{\left(2\pi\frac{\Delta_\epsilon}{\lambda}\right)^2 {k_1}^2\, u(\theta,\phi)^2\, v(\theta,\phi)^{2k_1}\sin^2(\theta)\cos^{2k_0+2}(\theta)}$

[a] $u(\theta,\phi)=\sin(\theta)\cos(\phi)$.

[b] $v(\theta,\phi)=\sin(\theta)\sin(\phi)$.

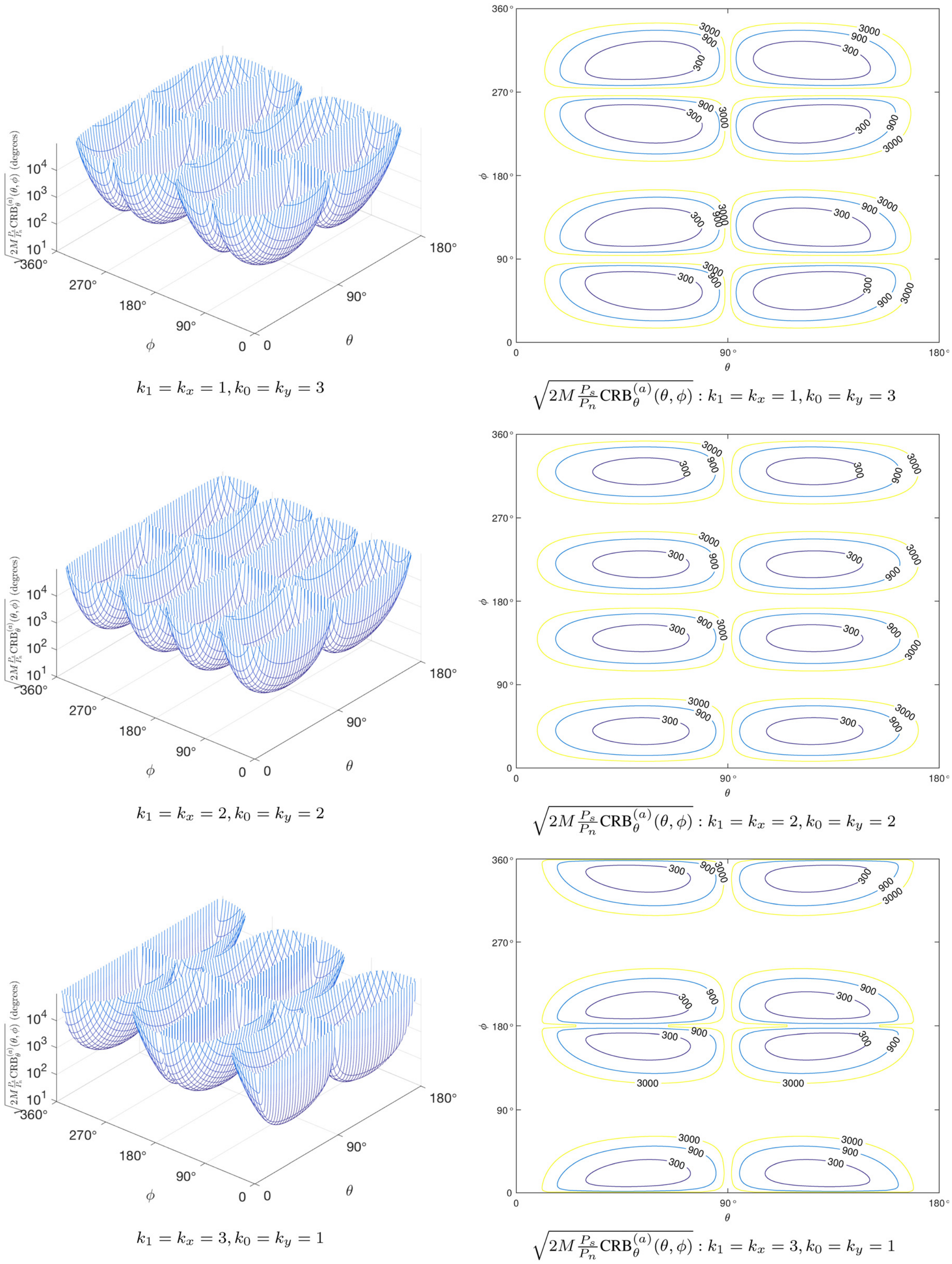

FIG. 2. (Color online) Configuration (a), i.e., x axis–oriented sensor at (λ/2,0,0) and y axis–oriented sensor at (0,0,0), and $\Delta_\epsilon/\lambda = \frac{1}{2}$, under the constraint of $k_1 + k_0 = 4$.

dotted) curve in Fig. 4(a) [Fig. 4(b)]} has the worst cumulative histogram. This case concentrates most directivity along the x axis (y axis) at the expense of the directivity along the y axis (x axis): Not only is the inter-sensor aperture along the x axis (y axis), the x-oriented (y-oriented) figure-8 sensor is allowed an order of 3 versus the y-oriented (x-oriented) sensor's order of 1. This observation would suggest that distributing the directivity over more Cartesian axes would lead to a better CRB cumulative histogram.

(v) In configuration (c), the inter-sensor spacing favors neither horizontal axis over the other horizontal axis. Instead, the directivity along the x and y axes depends only on (k_0,k_1). Among the three curves plotted for this

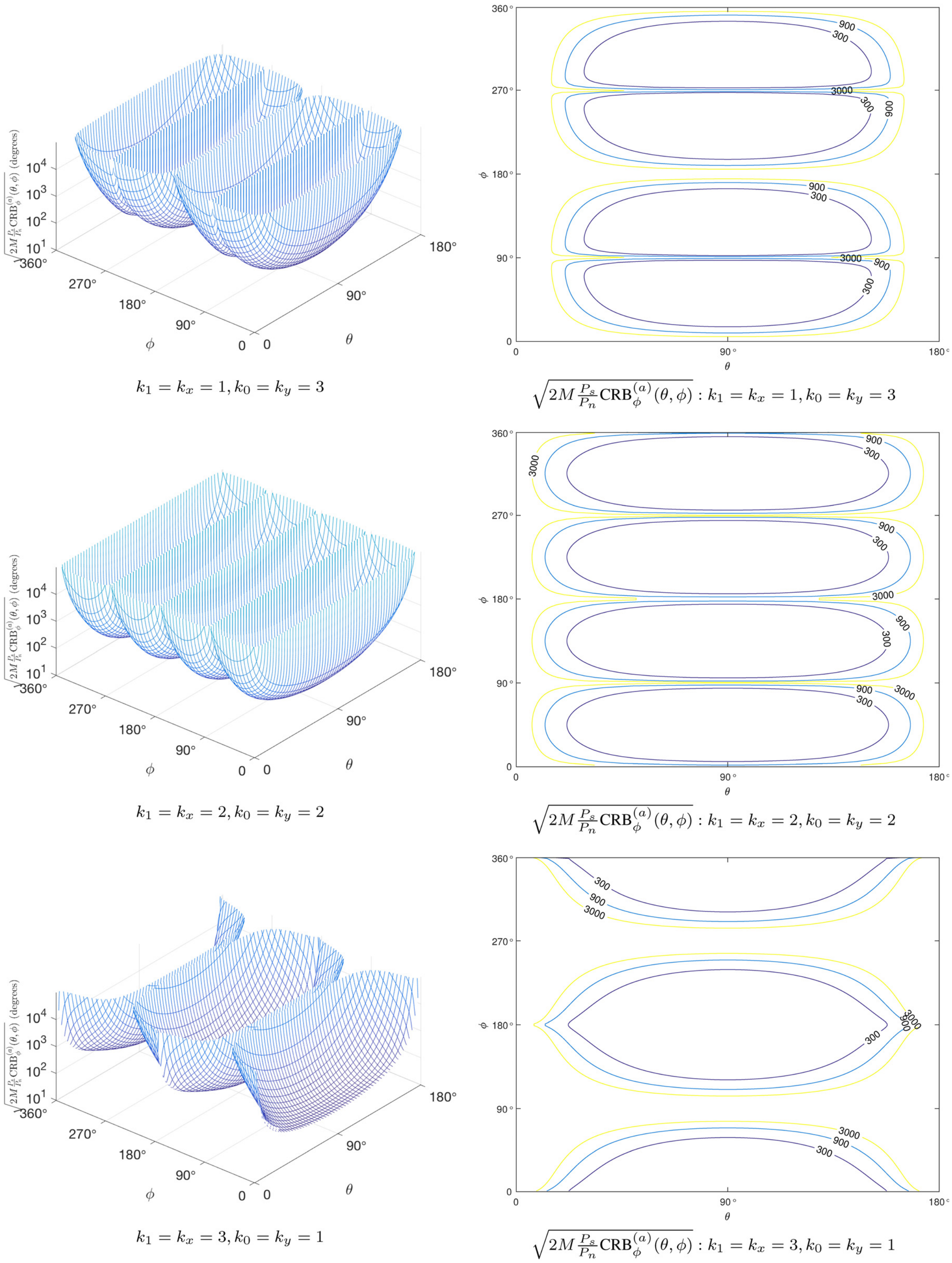

FIG. 3. (Color online) Configuration (a), i.e., x axis–oriented sensor at (λ/2,0,0) and y axis–oriented sensor at (0,0,0), and $\Delta_\epsilon/\lambda = \frac{1}{2}$, under the constraint of $K_1 + k_0 = 4$.

configuration (c), the $(k_0,k_1) = (2,2)$ case most evenly distributes the directivity between the x and y axes; it is this case that gives the best cumulative histograms, thereby reinforcing the earlier mentioned point that more evenly distributed directivity gives the best CRB performance.

(vi) For configurations (d) and (h), the sensor at the Cartesian origin (corresponding to k_0) offers no horizontal directivity. Moreover, both the other sensor (corresponding to k_1) and the inter-sensor axis favor the k_0 axis—i.e., the x axis for configuration (d), but the y axis for configuration (h). The three curves for configurations (d) and (h) differ by how much directivity to share between the vertical axis and the k_0 axis. If more directivity is allocated to the vertical axis, the horizontal k_0 axis (already favored by the inter-sensor axis) would be less over-emphasized.

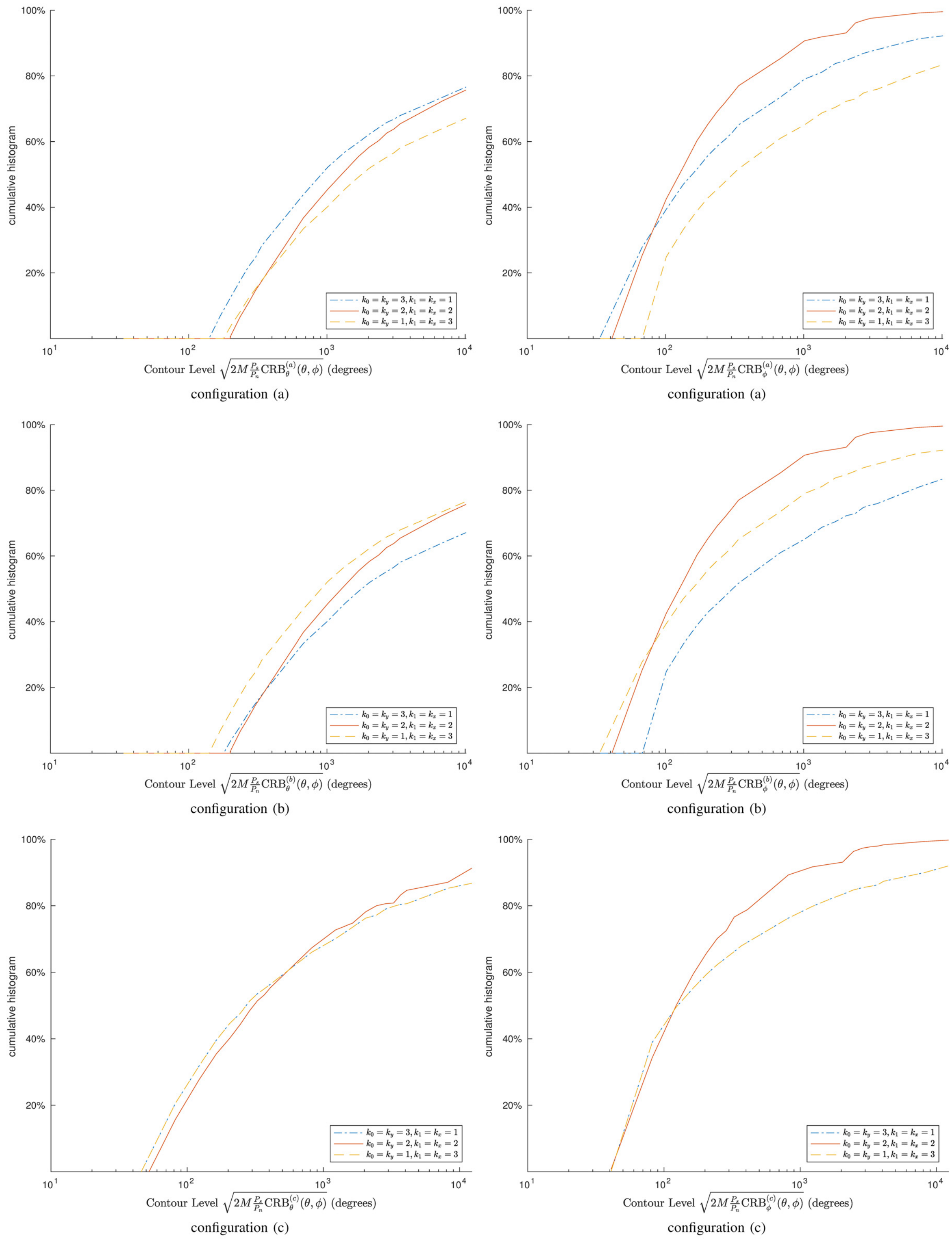

FIG. 4. (Color online) The CRB's cumulative histogram.

Indeed, this case leads to the best cumulative histogram. This echoes yet gain the aforementioned point that more evenly distributed directivity produces the best CRB performance.

(vii) For configurations (e) and (g), directivity is shared among all three axes, regardless of the specific numerical settings of k_0 and k_1, thereby leading to the three curves being close among themselves.

(viii) Configurations (f) and (i) enjoy vertical directivity, both from the k_0 sensor's vertical orientation and the inter-sensor axis also being vertical. The only horizontal directivity is provided by the k_1 sensor's horizontal orientation. Hence, a larger k_1 would less over-emphasize the vertical axis; this indeed gives the best cumulative histograms. This further strengthens the repeating observations here that

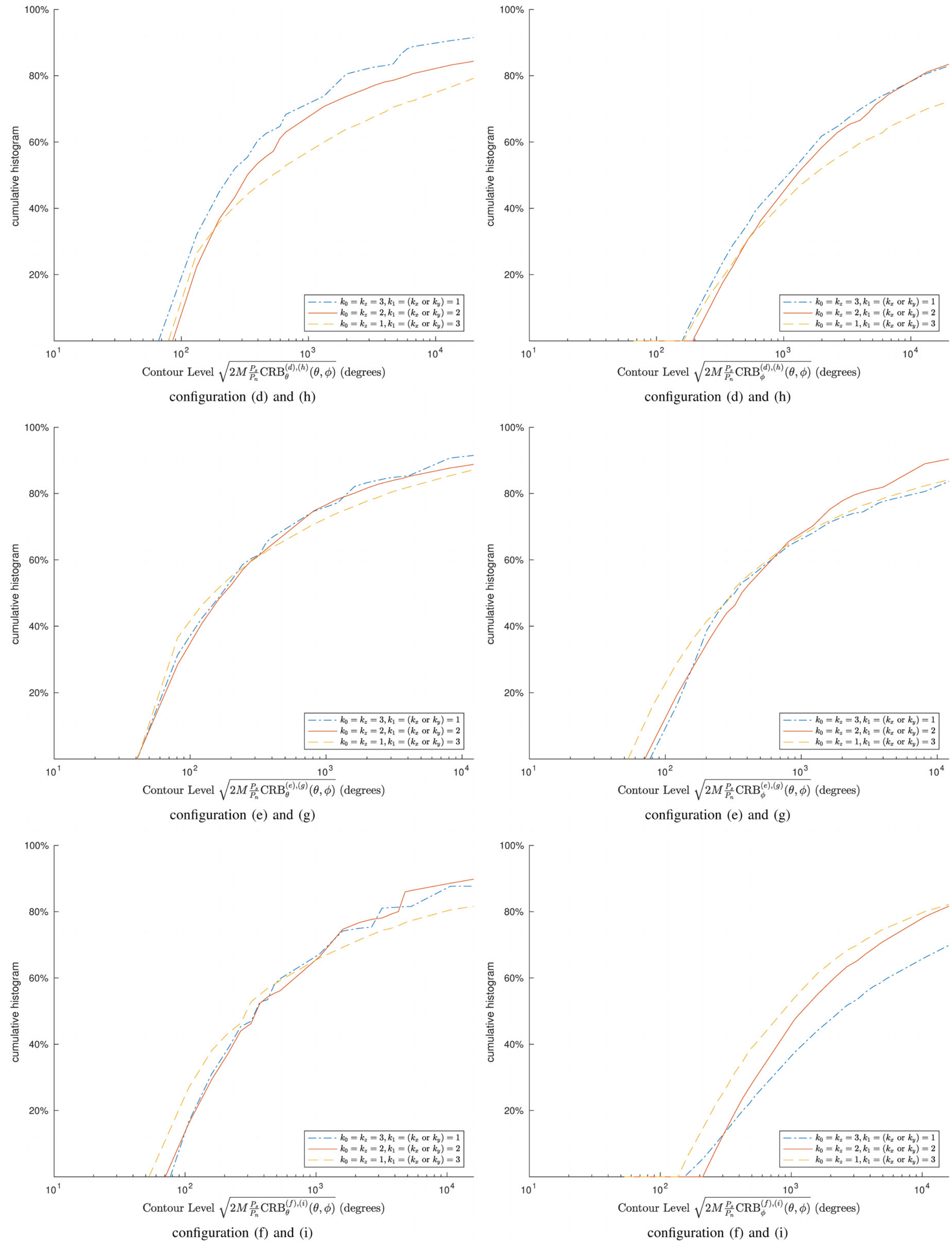

FIG. 4. (*Continued*)

more evenly distributed directivity leads to the best CRB performance.

V. MONTE CARLO SIMULATIONS

The statistical data model here will be same as that in Sec. IV. The Monte Carlo simulations use the following numerical settings: $\theta = 45°$, $\phi = 45°$, $\Delta_\epsilon/\lambda = \frac{1}{2}$.

Figure 5 plots the estimates' root-mean-square error (RMSE) versus the signal-to-noise ratio (SNR), where

$$\mathrm{RMSE} := \sqrt{\frac{1}{100}\sum_{i=1}^{100}\left(\widehat{\gamma}_i - \gamma\right)^2},$$

where $\gamma \in \{\theta,\phi\}$, and $\widehat{\gamma}_i$ symbolizes the estimation result of the ith Monte Carlo trial.

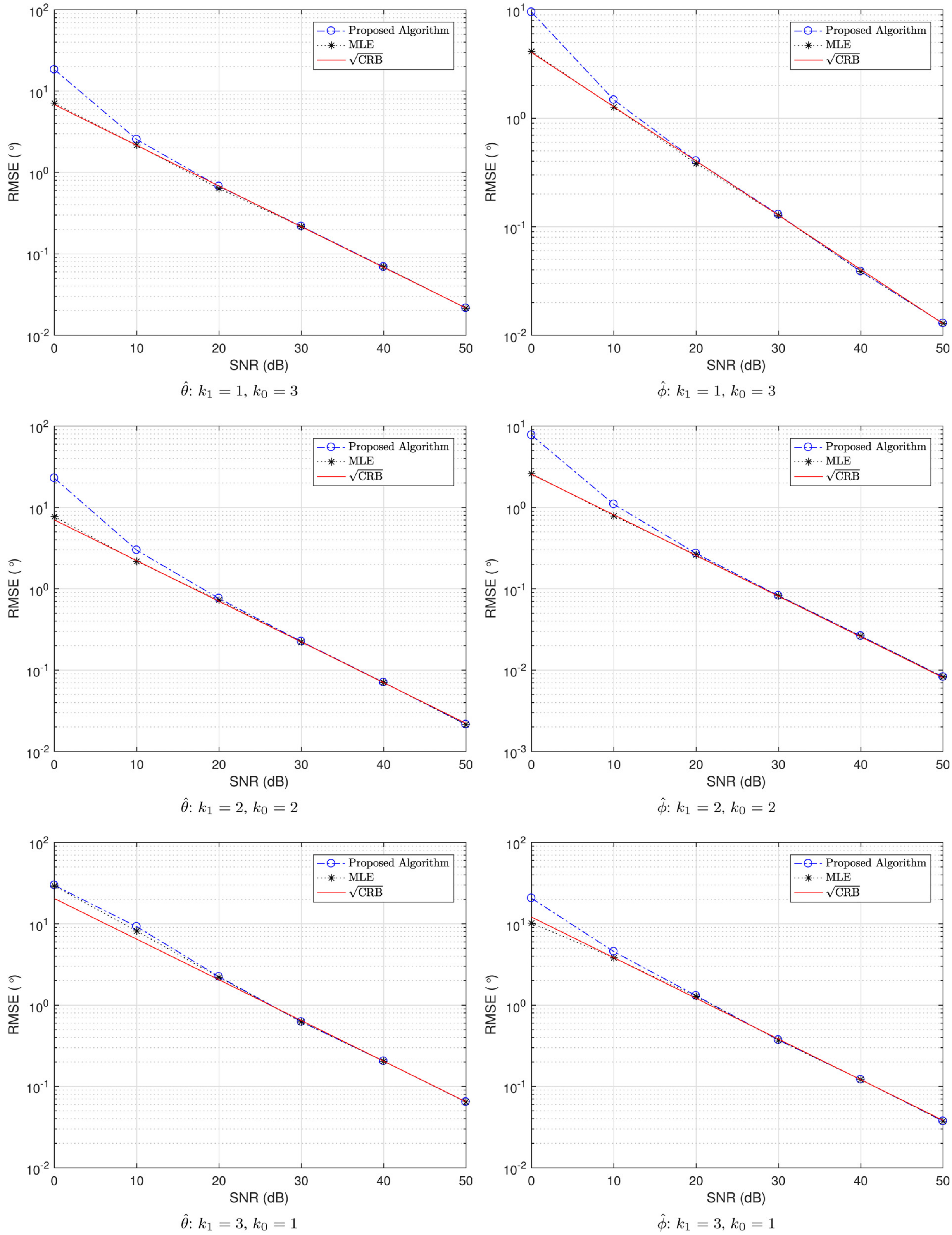

FIG. 5. (Color online) Monte Carlo simulations of proposed algorithm versus maximum likelihood estimation versus CRB for the estimator of elevation angle $\widehat{\theta}$ and azimuth angle $\widehat{\phi}$ using configuration (a) with the following settings: $M = 500$, $\theta = 45°$, $\phi = 45°$, $\Delta_x/\lambda = 1/2$.

Figure 5 clearly shows the proposed estimators to approach the CRB asymptotically as the signal-to-noise power increases.

Also plotted in Fig. 5 is the maximum likelihood estimator (MLE), which is a statistically efficient estimator (i.e., asymptotically approximates the error is also plotted CRB). The MLE data points indeed lay effectively on the CRB curves for $\mathrm{SNR} \geq 20\,\mathrm{dB}$, thereby verifying the correctness of the CRB curves. The deviation at small SNR values is probably exasperated by the nonlinear regions of inverse trigonometric functions.

The proposed estimators' RMSE performance is visually indistinguishable from the MLE's, for any SNR above 25 dB. At a more adverse (i.e., lower) SNR, the proposed estimators do admittedly incur larger RMSEs than the MLE; the proposed estimator requires much less prior information than does the MLE. The former needs no prior knowledge of the additive noise's probability density at each sensor, but the MLE does require this prior information. Moreover, the MLE requires an iterative optimization of the likelihood function. Such an iteration has many disadvantages: The iteration can be computationally burdensome for real-time applications; the iterative search requires a good initial estimate of the unknown parameter to start off the iteration to converge at the global optimum (instead of a local optimum).

VI. CONCLUSION

An orthogonal pair of figure-8 bi-directional sensors suffice for azimuth-elevation bivariate direction finding. For this, new algorithms have been advanced here in closed form, regardless of each sensor's respective order and the two sensors' separation. Moreover, CRB analysis suggests that the DOA estimates would generally be the most precise if the sensors' directivity and the inter-sensor axial directivity are evenly distributed along the three Cartesian coordinates.

ACKNOWLEDGMENTS

The authors would like to thank Dr. William C. Kirkpatrick Alberts, Dr. Yang Song, and Dr. Dominic M. Kitavi for useful discussions.

[1]Incidentally, *first*-order figure-8 sensors have been used in a collocated and perpendicular *triad*, called a "tri-axial velocity-sensor," or a "velocity-sensor triad," or a "vector sensor," or a "vector hydrophone." For comprehensive reviews of the tri-axial velocity-sensor literature, please consult Awad and Wong (2012), Tam and Wong (2009), and Wu and Wong (2012). *Higher*-order figure-8 sensors have also been used in a collocated and perpendicular *triad* in Song and Wong (2012).

[2]This endnote briefly reviews the eigen-based parameter estimator. Consider a wireless signal $\{s(m), \forall m = 1, 2, \ldots, M\}$ impinging upon two sensors, which produces a 2×1 data vector of $\mathbf{z}(m) = s(m)\mathbf{a} + \mathbf{n}(m)$ at the mth time instant. The 2×1 vector $\mathbf{a}$ here represents sensor-pair's array manifold, and $\{\mathbf{n}(m), \forall m = 1, 2, \ldots, M\}$ represents the additive noise at the sensor-pair and is spatially uncorrelated between the two sensors. From M such time instants of data, form a 2×2 spatial covariance matrix of $\widehat{\mathbf{C}} := (1/M)\sum_{m=1}^{M}\mathbf{z}(t_m)[\mathbf{z}(t_m)]^H$, where the superscript "^{H}" refers to the Hermitian operator. Suppose also that $\{s(t), \forall t\}$ and $\{\mathbf{n}(t), \forall t\}$ are each temporally stationary and are not cross-correlated between them. Consequentially, $\widehat{\mathbf{C}} \approx \mathbf{C} = P_s\mathbf{a}\mathbf{a}^H + P_n\mathbf{I}$, where P_s symbolizes the impinging signal's power, P_n represents to each sensor's noise power, and $\mathbf{I}$ denotes a 2×2 identity matrix. The 2×2 matrix $\widehat{\mathbf{C}}$ is Hermitian, and asymptotically approaches $\mathbf{C}$ as $M \to \infty$. Moreover, $\widehat{\mathbf{C}}$ has a 2×1 principal eigenvector asymptotically equal to $c\mathbf{a}$, where c could be any complex-valued scalar of a magnitude of $1/\|\mathbf{a}\|$ and is algebraically independent of $\mathbf{a}$. Hence, the principal eigenvector of the sampled data-covariance matrix $\widehat{\mathbf{C}}$ is approximately $c\mathbf{a}$.

[3]The three configurations of (c),(e),(g) allow closed-form eigen-based estimation of the bivariate DOA *only if* $k_0 = k_1$. Section II E will explain why. Common to these three configurations (and only these three configurations) is that η_1, η_2, and μ together do not have three distinct values in the array manifold of Eq. (1).

[4]If the two figure-8 sensors are spatially collocated (i.e., $\Delta_\epsilon = 0$), the nine configurations of Fig. 1 will reduce to only three configurations: Configuration (a), (b), (c): $\eta_1 = u$, $\eta_2 = v$; Configuration (d), (e), (f): $\eta_1 = u$, $\eta_2 = w$; Configuration (g), (h), (i): $\eta_1 = v$, $\eta_2 = w$. This is because there would be no displacement axis between the two collocating sensors. The steering-vector estimate of (6) would then correspondingly simplify to

$$\widehat{\mathbf{a}}_{\zeta_1,\zeta_2} \approx c\mathbf{a}_{\zeta_1,\zeta_2} = c\begin{bmatrix}\eta_1^{k_1}\\ \eta_2^{k_0}\end{bmatrix},$$

which is entirely real-valued except for the unknown complex-valued scalar of c. In order to eliminate the unknown c, form

$$\widehat{\left(\frac{\eta_1^{k_1}}{\eta_2^{k_0}}\right)} = \frac{[\widehat{\mathbf{a}}_{\zeta_1,\zeta_2}]_1}{[\widehat{\mathbf{a}}_{\zeta_1,\zeta_2}]_2}.$$

This gives one real-valued constraint, but there exists two real-valued unknown scalars in θ and ϕ, thereby forming an under-determined situation. Therefore, if the two figure-8 sensors are spatially collocated, bi-axial direction finding would not be viable.

[5]If the two sensors' locations are inter-changed, The complex exponential factor in Eq. (1) would move from the first entry to the second entry. Consequentially, Eq. (7) would have its complex exponent complex-conjugated; and Eq. (9) would have its right side negated. Therefore, the only modification to the subsequent estimation formulas is to re-define $F_2(k_1,k_0,\theta,\phi)$ as

$$F_2(k_1, k_0, \theta, \phi) := -\frac{\lambda}{2\pi\Delta_\epsilon}\angle\left(\mathrm{sgn}\left(\frac{\eta_1^{k_1}}{\eta_2^{k_0}}\right)\frac{\left[\widehat{\mathbf{a}}_{\zeta_1,\zeta_2}^{(\epsilon-\text{axis})}\right]_1}{\left[\widehat{\mathbf{a}}_{\zeta_1,\zeta_2}^{(\epsilon-\text{axis})}\right]_2}\right).$$

[6]Nearly pure-tone acoustic signals could arise naturally, e.g., in rotary-wing aircraft or in a ship/submarine's propeller. Pure-tone signals can also be obtained by decomposing wideband signals into distinct frequency-bins (e.g., via a short-time discrete Fourier transform). Each frequency-bin's performance would be given by the Cramér-Rao lower bound (CRLB) analysis keyed to that frequency-bin.

Awad, M. K., and Wong, K. T. (**2012**). "Recursive least-squares source-tracking using one acoustic vector-sensor," IEEE Trans. Aerosp. Electron. Syst. **48**(4), 3073–3083.

Bastyr, K. J., Lauchle, G. C., and McConnell, J. A. (**1999**). "Development of a velocity gradient underwater acoustic intensity sensor," J. Acoust. Soc. Am. **106**(6), 3178–3188.

Beavers, B. R., and Brown, R. (**1970**). "Third order gradient microphone for speech reception," in *Convention of the Audio Engineering Society*, May 4–7, Los Angeles, CA, pp. 636–640.

Brouns, A. J. (**1981**). "Second-order gradient noise-cancelling microphone," in *IEEE International Conference on Acoustics, Speech, and Signal Processing*, March 30–April 1, Atlanta, GA, pp. 786–789.

de Bree, H. E. (**2003**). "An overview of microflown technologies," Acta Acust. Acust. **89**(1), 163–172.

de Bree, H. E., Basten, T., and Yntema, D. (**2008**). "A single broad banded 3D beamforming sound probe," in *German Annual Conference on Acoustics*, March 10–13, Dresden, Germany.

de Bree, H. E., and Wind, J. (**2010**). "A particle velocity gradient beam forming system," in *24th National Conference on Noise Control Engineering*, April 19–21, Baltimore, MD.

Hines, P. C., Rosenfeld, A. L., Maranda, B. H., and Hutt, D. L. (**2000**). "Evaluation of the endfire response of a superdirective line array in simulated ambient noise environments," in *MTS/IEEE Oceans Conference*, September 11–14, Providence, RI, pp. 1489–1494.

Huang, Y., and Benesty, J. (**2004**). *Audio Signal Processing for Next-Generation Multimedia Communication Systems* (Springer, New York).

Klinke, S. A. (**2003**). "Directional microphone arrangement and method for signal processing in a directional microphone arrangement," U.S. patent application 2003/0174852 (September 18, 2003).

Klinke, S. A. (**2006**). "Directional-microphone and method for signal processing in same," U.S. patent 7,120,262 (October 10, 2006).

McConnell, J. A., Lauchle, G. C., and Gabrielson, T. B. (**2001**). "Two geophone underwater acoustic intensity probe," U.S. patent 6,172,940 B1 (January 9, 2001).
Miles, R. (**2005**). "High-order directional microphone diaphragm," U.S. patent 6,963,653 (November 8, 2005).
Olenko, A. Y., and Wong, K. T. (**2013**). "Noise statistics of a higher order directional sensor, realized by computing finite differences spatially across multiple isotropic sensors," IEEE Trans. Aerosp. Electron. Syst. **49**(4), 2792–2798.
Olenko, A. Y., and Wong, K. T. (**2015**). "Noise statistics across the three axes of a tri-axial velocity sensor constructed of pressure sensors," IEEE Trans. Aerosp. Electron. Syst. **51**(2), 843–852.
Olson, H. F. (**1941**). "Electroacoustical signal translating apparatus," U.S. patent 2,301,744 (May 31, 1941).
Olson, H. F. (**1957**). *Acoustical Engineering*, 2nd ed. (Van Nostrand, Princeton, NJ).
Raangs, R., Druyvesteyn, W. F., and de Bree, H. E. (**2001**). "A low cost intensity probe," in *110th Audio Engineering Society Convention*, Amsterdam, The Netherlands.
Rosenfeld, M. M. (**1962**). "Pressure gradient transducers," U.S. patent 3,068,328 (December 11, 1962).
Song, Y., and Wong, K. T. (**2012**). "Closed-form direction finding using collocated but orthogonally oriented higher-order acoustic sensors," IEEE Sens. J. **12**(8), 2604–2608.
Song, Y., Wong, K. T., and Li, Y. (**2015**). "Direction finding using a biaxial particle velocity sensor," J. Sound Vib. **340**, 354–367.
Tam, P. K., and Wong, K. T. (**2009**). "Cramér-Rao bounds for direction finding by an acoustic vector-sensor under non-ideal gain-phase responses, noncollocation, or non-orthogonal orientation," IEEE Sens. J. **9**(8), 969–982.
Warren, D. M. (**2008**). "Microphone array having a second order directional pattern," U.S. patent 7,471,798 (December 30, 2008).
Warren, D. M., and Thompson, S. C. (**2003**). "Microphone array having a second order directional pattern," U.S. patent application 2003/014283 (July 31, 2003).
Wiggins, A. M. (**1959**). "Higher order pressure gradient microphone system having adjustable polar response pattern," U.S. patent 2,896,189 (July 21, 1959).
Wiggins, A. M. (**1950**). "Second order differential microphone," U.S. patent 2,529,467 (November 07, 1950).
Wiggins, A. M. (**1951**). "Second order differential microphone," U.S. patent 2,552,878 (May 15, 1951).
Wu, Y. I., and Wong, K. T. (**2012**). "Acoustic near-field source localization by two passive anchor nodes," IEEE Trans. Aerosp. Electron. Syst. **48**(1), 159–169.